Energy 258 (2022) 124762

Contents lists available at ScienceDirect

Energy

journal homepage: www.elsevier.com/locate/energy

Assessment of HVAC system operational fault impacts and multiple faults interactions under climate change

Fangliang Zhong*, John Kaiser Calautit, Yupeng Wu

Department of Architecture and Built Environment, University of Nottingham, United Kingdom

ARTICLE INFO

Article history:
Received 20 December 2021
Received in revised form
21 June 2022
Accepted 5 July 2022
Available online 14 July 2022

Keywords:
Fault impact analysis
Multiple faults
HVAC
Future climate scenarios
Building performance simulation

ABSTRACT

The effect of climate change on heating, ventilation and airconditioning (HVAC) system performances has become prominent, and HVAC fault impacts may also vary with climate change. This paper evaluates the impacts of HVAC operational faults on system energy and occupant thermal comfort under the current, 2030s and 2050s climates using a validated model. The energy and thermal comfort impact indicators were proposed to rank single and multiple faults under each climate period. Supply fan stuck at maximum speed, and the combinations associated with this fault were ranked first in energy and thermal comfort rankings, respectively. Based on the investigations of multiple faults interactions, it is found that the synergetic/antagonistic effect of multiple faults combinations can lead to a significantly higher/lower combined impact than any single fault impact among the combination when the single faults present opposite impacts. Moreover, heating coil supply air temperature sensor negative bias, and the combination of thermostat positive offset and outdoor air damper stuck fully open led to the most increase system total electricity by 34.3 GJ and 35.3 GJ from current to 2050s period. The results are useful for researchers to prioritise the faults with significant impacts for developing fault detection and diagnosis framework.

1. Introduction and literature review

According to the World Energy Outlook 2020 [1], buildings accounted for 30.7% of the world's total final energy consumption. Heating, ventilation, and air conditioning (HVAC) systems were responsible for up to 57% of the end energy use for commercial and residential buildings [2]. Hence, a large number of research work was conducted to develop energy-efficient and sustainable HVAC systems, such as cooling and heating systems powered by solar energy [3] and geothermal energy [4]. In addition, advanced HVAC controls have been widely applied to the systems, which include vision-based occupant behaviors detection [5], occupant thermal comfort personalised control strategy [6], etc. However, the design expectation of energy-efficient HVAC systems is still hardly met when the systems are put into operation. One of the major factors affecting the energy performance of HVAC systems is the occurrences of faults during their lifecycle. According to a survey in California, 65% of residential air conditioning units and 71% of commercial air conditioning units were involved with faults [7]. Typical HVAC faults can be mainly classified into three groups: control faults, sensor faults and equipment faults [8]. A large number of operational faults existing in HVAC systems leads to an additional 20% or even more of HVAC energy consumption [2]. Meanwhile, the degraded HVAC equipment also influences the indoor occupant thermal comfort and might reduce the productivity of occupants in workplaces. As a result, increasing demand for the development of robust fault detection and diagnosis (FDD) methods for HVAC systems has arisen because FDD methods are indicated to reduce HVAC energy consumption by 10–40% [9], and these methods can be mainly categorised into three types: rule-based methods [10], model-based methods [11] and data-driven methods [12].

To support the development of FDD methods for HVAC systems, especially data-driven methods, fault impact assessments are needed for the following reasons: First, there are usually tens of faults occurring during the lifecycle of an HVAC system, and each of them has a different influence on system energy consumptions, occupant thermal comfort, etc. A fault impact analysis on these faults can help FDD developers identify the prioritisation of faults to be focused on in an FDD framework since an FDD method may

* Corresponding author.
E-mail addresses: Fangliang.Zhong@outlook.com (F. Zhong), john.calautit1@nottingham.ac.uk (J.K. Calautit).

https://doi.org/10.1016/j.energy.2022.124762

not be able to detect and diagnose all kinds of faults with the same high detection and diagnosis accuracies. For instance, the predicted accuracy for all the 19 faults covered in the study of [13] varies from 80% to nearly 100%. Thus, maximising the detection and diagnosis accuracies for the faults with substantial impacts and compromising on the accuracies for the faults with considerably less impacts should be an objective for optimising the FDD framework. Second, multiple faults existing in an HVAC system is a common case in reality. To investigate the interactions among multiple faults and the combined fault effects, it is critical to perform a fault impact analysis on individual fault and multiple fault cases [14].

1.1. Literature review and research gap

Fault modeling [15,16] and simulation [17] using whole building performance simulation (BPS) programs, such as EnergyPlus [18], is a robust and effective approach to support the assessment of HVAC operational fault impacts. Regarding the BPS, the validation of BPS models is an essential step to verify the fitness between the BPS model and the corresponding real building. Reddy et al. [19] proposed a five-step methodology to calibrate BPS models to fit the measured energy utility data and introduced 'goodness-of-fit' (GOF) as a statistical indicator to represent the fitness degree of the models to corresponding real buildings. The GOF indicator was expressed by the coefficient of variation of root mean square error (CV(RMSE)) and normalised mean bias error (NMBE) [20].

Based on the whole BPS program, HVAC fault impacts can be evaluated under any specified climatic conditions and analysed thoroughly according to the simulation outputs, including system energy, occupant thermal comfort, etc. Previous fault impact studies can be divided into two groups: single fault only impact analysis and combined single and multiple faults impact analysis. With respect to single fault impact analysis, most studies focused on the fault impact at the whole-building or system level. Lee and Yik [21] presented the influences of sensor and actuator faults on variable air volume (VAV) system energy end usages under the climate of Hongkong. Basarkar et al. [22] simulated the impacts of four single faults on the VAV system energy under the mixed humid and cold climates. Zhang and Hong [23] investigated the effect of sensor biases and filter fouling on HVAC system heating and cooling energy and occupant thermal comfort under hot humid, marine and cold climates. Lu et al. [24] analysed the effects of 359 fault cases on various impact indicators, including energy usage, thermal comfort levels, operational cost, ventilation metrics, etc., under the cold climate. Huang et al. [25] evaluated the annual energy variations of chiller and boiler plants and thermal unmet hours caused by 13 control-associated faults. In addition, some of the literature evaluated the fault impacts at the component level. Cheung and Braun [26] assessed the influences of four chiller faults on the energy consumption of chiller and cooling towers under the hot humid, and hot dry climates. Moreover, the impacts of refrigerant-related single faults on cooling capacity and coefficient of performance (COP) for split system air conditioners [27] and heat pumps [28] were both explored using laboratory experiments. However, none of these studies focused on the impacts of multiple faults.

As for the studies concerning both single and multiple faults, Ginestet, Marchio and Morisot [29] explored the effects of individual faults from the valve, damper and sensors and combinations of them on heating coil energy usage and indoor air quality. Wang and Hong [30] assessed the influences of thirteen single faults and only two multiple faults cases on HVAC end-use energy for a VAV system under a cold climate. Li and O'Neill [31] evaluated the effects of 129 fault scenarios, including both single and multiple faults cases, on VAV system energy usage and occupant thermal comfort under the mixed humid, hot humid, marine and cold climates. Lu et al. [17] simulated the impacts on HVAC energy usage and ventilation performance induced by individual and multiple faults of CO_2 and airflow sensors for a demand-controlled ventilation system. Similarly, Yoon et al. [32] studied the influences of AHU and chiller sensor offsets and combinations of them on system end-use energy, COP and thermal comfort under the marine, cool dry, hot humid, cold and mixed humid climates. However, none of these studies investigated the underlying interactions among multiple faults.

Regarding the studies concerning multiple faults interactions, Zhou et al. [33] and Hu et al. [34] both carried out an experimental investigation into the interactions among multiple refrigerant-related faults on system performances, such as COP and cooling capacity. However, none of these studies considered the fault impacts under a changing climate.

In summary, previous fault impact studies covered a wide variety of single faults, but the combinations of multiple faults explored were still limited. Some of the multiple faults work investigated interactions among multiple faults, however, they only included several refrigerant-related faults and focused on the impacts on system performance metrics, such as COP. There is still a lack of literature exploring the interactions among a wider range of multiple faults, such as the interactions among sensor and actuator faults, and assessing the impacts on whole-building scale performance metrics, such as system total electric and gas energy usages and occupant thermal comfort. In addition, previous studies evaluated fault impacts under a number of climate zones, but the climate data used in these studies were based on historical climate periods. The impacts of HVAC operational faults may vary with changing climate conditions. The negative impacts of global warming are now an inevitable fact, and the Intergovernmental Panel on Climate Change (IPCC) [35] predicted that the variation of global mean surface temperature would increase by the ranges between 0.4 − 1.6 °C and 1.4–2.6 °C from a benchmark period of 1986–2005 to the mid of this century. Thus, to the authors' best knowledge, there is still a gap for fault impact analysis based on changing climate data from different periods, which is also worth to be performed under the background of climate change.

1.2. Aims and objectives

Based on the above comprehensive review of previous fault impact studies, the impacts of single and multiple HVAC faults on whole-building scale performance metrics under future climate scenarios have not yet been evaluated, and the potential effect of climate change on single and multiple fault impacts and multiple faults interactions has not yet been explored. Hence, the present study evaluates the impacts of typical operational faults, including control, sensor, VAV terminal unit, direct-expansion (DX) packaged air conditioning unit, etc., and their combinations for one of the most common HVAC systems in commercial buildings, VAV system, under the current and future (2030s and 2050s) climate conditions. It also explores the variations in fault impacts, in terms of system energy consumptions and occupant thermal comfort, and multiple faults interactions across different climate periods. A U.S. Department of Energy (DOE) prototype medium-sized office building model was used as a case study and verified against the DOE source results. The fault cases were developed following the modeling approaches described in previous studies [14–16] and simulated using a widely used whole BPS tool, EnergyPlus.

The main contributions of this study are summarised as follows:

- The energy and thermal comfort impact indicators, based on the fault impact variations from the baseline normal case for each single or multiple faults combination, were proposed to rank the

single and multiple faults in terms of system energy consumptions and occupant thermal comfort under each climate period. In addition, the cause and effect analysis for the top-ranked faults were provided.
- Based on the differences between actual combined effects of multiple faults and algebraic sums of these fault impacts for every single fault involved in the multiple faults case, the interactions among multiple faults were divided into two categories: synergetic effect and antagonistic effect. The causes for these effects were explained, and climate change's influence on these effects was analysed.
- The variations in single and multiple fault impacts across different climate periods were evaluated, and the single and multiple faults with substantial variations from current to 2030s and from current to 2050s were highlighted.

2. Fault modeling method

The general workflow for evaluating HVAC fault impacts and multiple faults interactions under current and future climate periods is illustrated in Fig. 1a, which mainly consists of two parts, i.e., fault modeling and fault simulation. In this section, the fault modeling methods [15,16] used in this study are briefly described and further details of the modeling method for each fault can be found in Supplementary Material. According to the fault modeling methods from Ref. [14], fault models can be developed independently and introduced into building models using a variety of whole BPS tools, in this case, EnergyPlus.

The steps for developing fault models are illustrated in Fig. 1b. Firstly, the faults and their corresponding intensities were defined. Next, the associated parameter(s) in EnergyPlus, as shown in Table 1, were linked to each fault, and the fault impact on the parameter(s) was formulated using Python [36]. After the fault impact formulation, the fault models were then introduced into the EnergyPlus building model. This paper focuses on developing fault models under five categories, including control, sensor, DX packaged air conditioning unit, VAV terminal unit, and other faults [15]. The definitions of intensities, their ranges, and the associated parameters in EnergyPlus for these faults are described in Table 1. The details of the fault simulation method are presented in Section 3.

3. Fault simulation method

3.1. The case study building and HVAC system

The DOE EnergyPlus commercial prototype medium office building model [38], commonly used to evaluate the energy performances of commercial buildings under different climate zones [39–41], was used as the case study for assessing the fault impacts under current and future weather conditions. This particular model

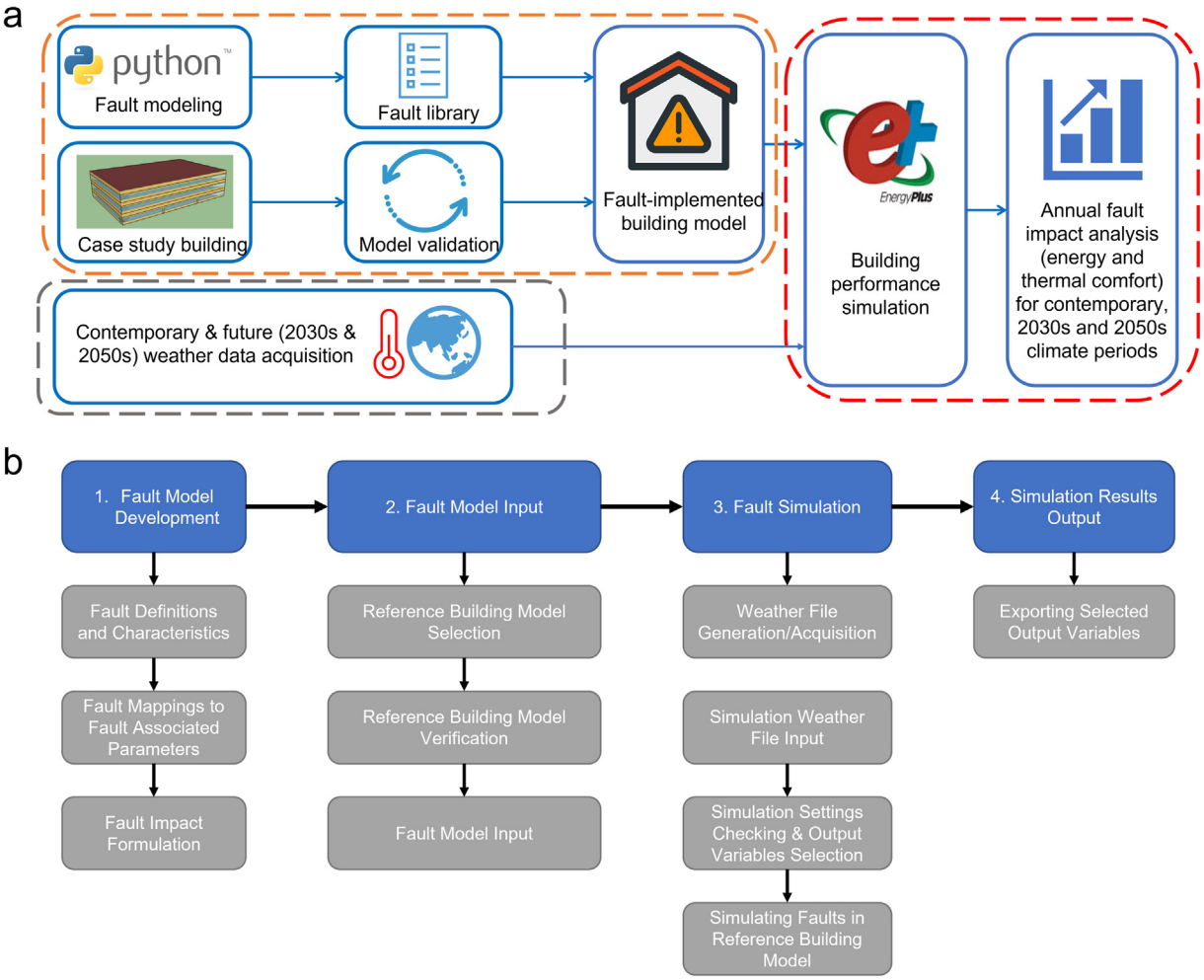

Fig. 1. (a) A general overview of the methodology flowchart for evaluating HVAC fault impacts under current and future climate periods; (b) detailed fault modeling and simulation processes.

Table 1
Descriptions of fault characteristics [14–16].

Fault name	Fault intensity	Fault intensity range	Associated parameters
Control faults			
No overnight setback	Overnight setback is set up or not	0 or 1	Heating/cooling schedules setpoints
Extended morning setback	Hours that the setpoint for the occupied period is extended forward in the morning	0–3 h	Time for ending the unoccupied period in heating/cooling schedules
Delayed evening setback	Hours that the setpoint for the occupied period is delayed in the evening	0–3 h	Time for starting the unoccupied period in heating/cooling schedules
Occupant manual changes of setpoint	The temperature threshold that occupants will alter the thermostat setpoints and the degree(s) of setpoints altered	User-defined	Time when the setpoint is altered and the altered setpoint added to heating/cooling schedules
Sensor faults			
Cooling/heating coil SA temperature sensor bias	Sensor offset in coil SA temperature	±4 °C	Fault availability and severity schedules, coil/controller/thermostat object name and type, as well as reference sensor offset [37]
Economizer OA temperature sensor bias	Sensor offset in OA temperature	±4 °C	
Economizer return air (RA) temperature sensor bias	Sensor offset in RA temperature	±4 °C	
Thermostat offset	Thermostat offset in zone air temperature	±3 °C	
Packaged air conditioner faults			
Supply fan motor efficiency degradation	The percentage of fan motor efficiency reduction	0–30%	Fan total efficiency in fan objects
Supply fan stuck at a fixed speed	Fan airflow rate stuck percentage	0–100%	EMS actuator: fan air mass flow rate
OA damper stuck	OA damper stuck position percentage	0–100%	Minimum and maximum OA fraction schedules
OA damper leakage	The ratio of the leaked OA flow rate to the OA flow rate at the full operation condition	0–40%	Minimum OA fraction schedules
VAV terminal unit faults			
VAV reheat coil complete failure	VAV reheat coil completely broken down or not	0 or 1	Reheat coil availability schedule(s)
Other faults			
Supply air duct leakage	The ratio of the leaked airflow rate to the supply airflow rate	0–30%	Constant downstream leakage fraction

has also been utilised in numerous works in the field, such as for the evaluation of conventional air-conditioning units [42] and novel cooling technologies [43]. Furthermore, it has been used for assessing HVAC fault impacts [31] and generating fault data to support the development of data-driven FDD methods [44]. In addition, the building model used in this study complies with ASHRAE 90.1–2004, 62.1–2004, and 62–1999 standards. Detailed descriptions of the reference model development and modeling strategies can be found in Ref. [38]. The model has been vetted by several national laboratories, technical committees, researchers, academics, industry professionals, and EnergyPlus users [38]. We have used this established reference building model and its inputs, which embodies an extensive collection of buildings research and knowledge, to avoid repeating the foundational work in this simulation study, which is not relevant to the main interest of this study.

The design day conditions of the original model were adjusted to the design day conditions of London [45], as detailed in Table 2. The medium office building is a three-storey building (Fig. 2a) with one core and four perimeter zones on each storey (Fig. 2b), as detailed in Table 2. The specifications and operation of the HVAC system are also detailed in Table 2.

3.2. Model verification with DOE source results

Due to the limitation of unavailable real measured energy data for this prototype building model, both the original model and the modified model with design day conditions of London were verified by comparing the simulation results with the DOE source simulation results [38]. As presented in Fig. 3, the two metrics, i.e., CV(RMSE) and NMBE for all the energy consumptions, except the heating coil gas energy, are lower than the absolute value of 1% for the present original model. The only large deviationfor the heating coil gas energy may be attributed to the version difference between the authors' EnergyPlus tool (version 9.3) and the model used for producing the source results by DOE (version 8.0). The use of EnergyPlus 9.3 is mainly due to the newly-developed fault modeling capability of the tool. In addition, the adjustment of design day conditions of the model led to higher errors, in terms of the two metrics, for all the energy consumptions. However, the CV(RMSE) and NMBE for these energy consumptions of the present original model and the modified model are both within the accepted ranges (15% and 5%) indicated in Ref. [20], and thus the case study building model is verified to be used for evaluating the HVAC fault impacts under different climate periods. It should be noted that further model developments and validations should be conducted in the future to ensure that the short-term and dynamic behaviours of the HVAC system and its components are captured.

3.3. Current and future climatic data

The fault simulations were implemented using a contemporary weather file and future weather files (the 2030s and 2050s) of London. The contemporary weather file was generated using Meteonorm 8 [47], a comprehensive meteorological program for generating contemporary and future weather data at most of the locations in the world in various formats of weather files. The contemporary weather data refers to the recent weather data based

Table 2
Overview of the HVAC system and control settings.

HVAC system configuration	
Air system type	VAV system
Cooling system type	DX packaged air conditioner
Heating system type	Gas furnace
Zone air distribution unit	VAV terminal unit
Design day conditions for system and zone sizings	Winter: dry-bulb temperature of −2.5 °C and corresponding dewpoint of −6.1 °C over 99.6% time; Summer: dry-bulb temperature of 28.3 °C and corresponding wet-bulb temperature of 18.6 °C below 0.4% time.
HVAC control settings	
System operation schedule	Weekdays: 6 a.m. to 10 p.m.; Saturday: 6 a.m. to 5 p.m.
Thermostat setpoint (occupied period)	Cooling: 24 °C; Heating: 21 °C
Thermostat setpoint (unoccupied period)	Cooling: 26.7 °C; Heating: 15.6 °C
Central system supply air temperature setpoint	Cooling: 12.8 °C; Heating: 15.6 °C

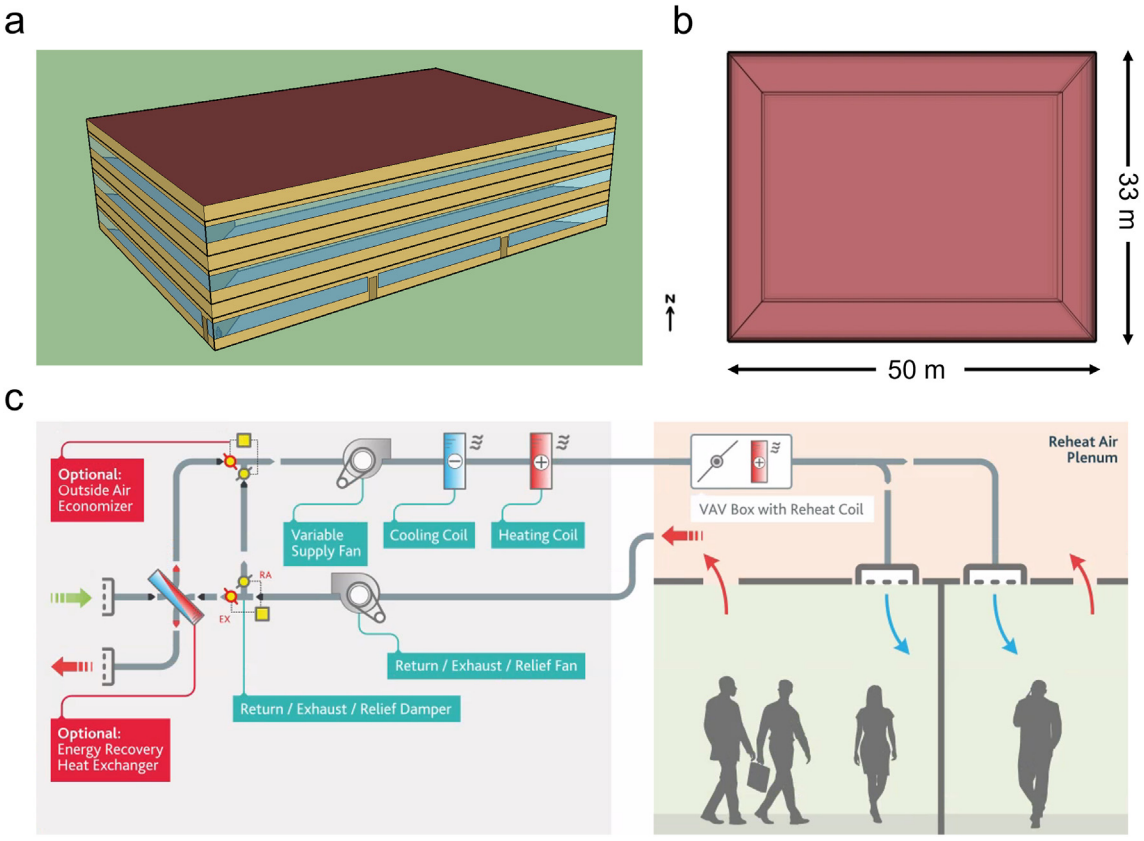

Fig. 2. (a) Case study medium office building model; (b) One core and four perimeter zones on the floor plan; (c) A typical VAV system with reheat coils and outdoor air economizer [46].

on radiation data from 1996 to 2015 and temperatures, wind, precipitation, etc., from 2000 to 2019 [47]. As for the future weather files, they were produced by Ref. [48] according to the IPCC medium emissions (A1B) scenario, which is a balanced scenario between the fossil fuel intensive scenario (A1FI) and the fossil fuel non-intensive scenario (A1T) [49]. The average monthly temperature for each same month between 1961 and 1990 at the 50th percentile was used as the baseline weather data, which represents medium predictions for future weather years [48]. Thus, two future weather files based on medium emissions (A1B) scenario under the 2030s and 2050s, respectively, were used to predict the fault impacts in future.

3.4. Fault simulation inputs and settings

The fault intensity for each fault introduced into the building model is presented in Table 3. Apart from the control faults, the other faults are assumed to occur in the core zone on the bottom floor or in the component serving the bottom floor to simplify the analysis of fault impacts. In terms of simulation settings, six time-steps per hour were used to calculate the zone heat transfer and load. The minimum and maximum number of warmup days for convergence were set to 6 and 25, respectively. As for the heat load calculation algorithms, polygon clipping [50] was used for the shadow calculation. Thermal Analysis Research Program (TARP)

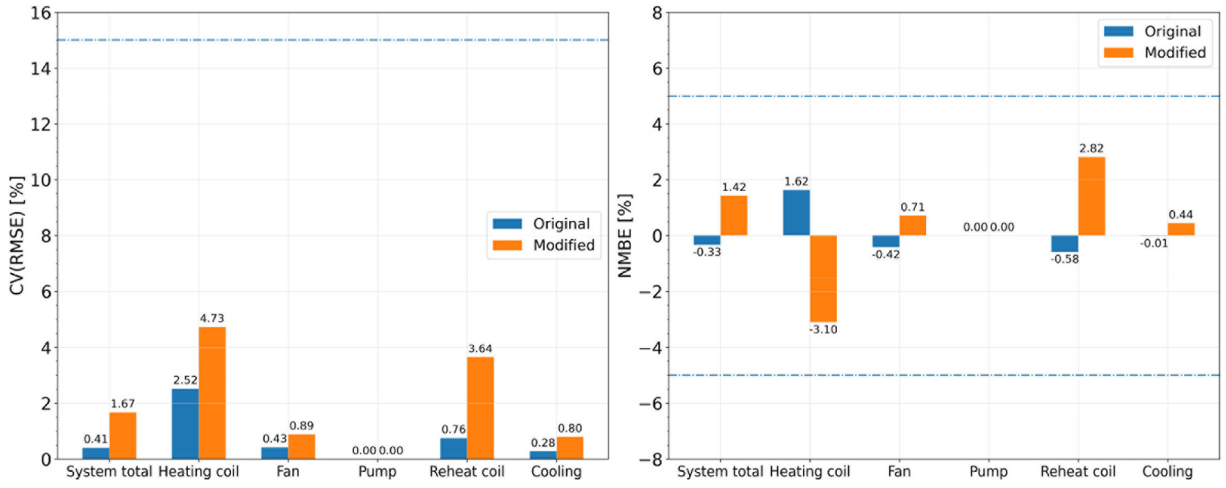

Fig. 3. CV(RMSE) and NMBE for system total and end-use energy of the present original model and the modified model, compared with the DOE source results.

Table 3
Fault intensity inputs for each fault model.

Fault name	Fault intensity
No overnight setback	1 (binary)
Extended morning setback	2 h
Delayed evening setback	2 h
Occupant manual changes of setpoint (heating season)	+2 °C when OA temperature is below −2.5 °C
Occupant manual changes of setpoint (cooling season)	−2 °C when OA temperature is above 26.2 °C
Cooling coil SA temperature sensor bias	±2 °C
Heating coil SA temperature sensor bias	±2 °C
Economizer OA temperature sensor bias	±2 °C
Economizer RA temperature sensor bias	±2 °C
Thermostat offset	±2 °C
Supply fan motor efficiency degradation	15%
Supply fan stuck at fixed speed	0.25, 0.5, 1
OA damper stuck	0, 50%, 100%
OA damper leakage	40%
VAV reheat coil complete failure	1 (binary)
Supply air duct leakage	30%

[51] was used to calculate the external and internal surface convections. Moreover, the conduction transfer function [50] was selected as the heat balance algorithm. The details of these governing equations can be found in Ref. [50]. Regarding evaluating the thermal comfort of occupants, the widely used Fanger comfort model [52] was selected.

3.5. Energy and thermal comfort impact ranking indicators

The energy end usages for each fault case E_{faulty} were compared with those of the baseline normal case E_{normal} to calculate the variation percentages δ in energy end usages between the fault and normal cases as follows:

$$\delta = \frac{E_{faulty} - E_{normal}}{E_{normal}} \tag{1}$$

The faults were ranked according to the maximum between the sum and the maximum value of the variations in energy end usages from the baseline normal case (Eqn. (2)), and the deviation φ in the mean of the PPDs for zones on the bottom floor from the baseline normal case (Eqn. (3)), respectively.

$$\delta_{rank} = max\left\{\sum_{i}^{n}\delta_i,\ \delta_{max}\right\} \tag{2}$$

where δ_{rank} is the percentage indicator used for ranking the faults;
δ_i is the percentage variation of each energy end usage;
δ_{max} is the maximum percentage variation among all types of energy end usages.

$$\varphi = \frac{1}{n}\left(\sum_{i=1}^{n} PPD_{i,f} - \sum_{i=1}^{n} PPD_{i,n}\right) \tag{3}$$

where $PPD_{i,f}$ represents the PPD for each thermal zone on the bottom floor under each fault case;
$PPD_{i,n}$ represents the PPD for the same thermal zone under the normal case;
n is the number of thermal zones on the bottom floor.

4. Results and discussion

Rankings and impacts of single and multiple faults are presented in Sections 4.1 and 4.2. The single and multiple faults were assumed to last across a whole year in order to evaluate the fault impacts in different months, and therefore the annual system energy end

usages and the yearly-average PPD for each zone of the bottom floor were used as evaluation indicators. The variations in fault impacts for each single or multiple faults combination across climate periods are assessed in Section 4.3.

4.1. Single fault impact and rankings

A general overview of the rankings for single faults, in terms of energy and thermal comfort impacts, is presented in Table 4. Each single fault is ranked based on the proposed energy and thermal comfort indicators from Eqns. (2) and (3) under the current, 2030s and 2050s periods. According to Table 4, the energy and thermal comfort impact ranks for most of the single faults remain the same among the three climate periods. The types of the top 6 faults in the energy impact ranking under three climate periods are the same, but the ranks for some of the top 6 faults vary across the climate periods. In terms of the thermal comfort impact ranking, eight out of the top 10 faults remain the same ranks while heating coil SA temperature sensor positive bias and OA damper stuck fully open descended from sixth and eighth under the current period to eighth and eleventh under the two future periods, respectively. Besides, no overnight setback showed the largest increase in the rank from eleventh under the current period to sixth under the 2030s period.

4.1.1. Cause and impact analysis for prioritised single faults

The energy and thermal comfort impacts of the top single faults in Table 4 under the current and 2050s period are shown in Figs. 4 and 5. The deviations of system energy end usages from the baseline normal case for the top 7 faults are illustrated in Figs. 4a and 5a. The deviations of the PPD from the baseline normal case for the top 10 faults are presented in Figs. 4b and 5b. Under the current period, most single faults demonstrate large discrepancies in energy impacts but show slight deviations in terms of the influence on thermal comfort, except for the supply fan stuck at maximum speed. This fault led to the most significant impact on system energy end usages and thermal comfort. Due to the largest requirement of supply air flow rate, which was achieved by increasing the amount of both return and outdoor air in the mixed air (Fig. 6a), it caused substantial increases in electricity usages of the air system total, reheating coils, cooling coil and fan by 109.72%, 111.41%, 40.49% and 226.95% (Fig. 4a), respectively. The only decrease for this fault occurred at the heating coil gas energy by 22.53% (Fig. 4a). In addition, the PPD was 9.70% higher than that of the baseline normal case (Fig. 4b). On the contrary, supply fan stuck at minimum speed led to decreases of 12−16% in the electricity usages but resulted in a considerable increase of 104.10% in heating coil gas energy (Fig. 4a). This effect was attributed to the use of full OA as the supply air at the minimum speed of the supply fan (Fig. 6b).

Apart from the supply fan stuck faults, no overnight thermostat setback indicated significant influences on the electricity usages of the air system total and reheating coils by +30.68% and +64.06%, respectively, but only caused a slight increase of 1.82% in cooling coil electricity usage (Fig. 4a). The difference in the electricity usage between the cooling coil and reheating coils can be explained by the setpoint differences of 2.7 °C and −5.4 °C between the unoccupied and occupied periods for cooling and heating, respectively (Table 2). In addition, another explanation for this difference is that the summer OA temperature in the evening is typically significantly lower than the thermostat setpoints in both occupied and unoccupied periods (Fig. 6c).

As for the OA damper stuck faults, OA damper stuck fully open resulted in an enormous increase of 230.22% in heating coil gas energy (Fig. 4a) due to the low winter outdoor air temperature. In contrast, the OA damper stuck fully closed led to a large rise of 51.37% in cooling coil electric energy (Fig. 4a) since the lower summer OA temperature than the zone air temperature in the morning of hot days or during the whole day of some summer days can contribute to the reduction in the mixed air temperature for the packaged air conditioners (Fig. 6c).

With respect to sensor faults, the positive bias in the cooling coil SA temperature sensor resulted in a lower actual temperature of supply air leaving the cooling coil and thus caused a rise in cooling coil electric energy of 15.55% (Fig. 4a). Meanwhile, this lower SA temperature led to a significant increase in heating coil gas energy

Table 4
Energy and thermal comfort impact rankings for single faults under each climate period.

Fault code	Fault type	Energy ranking			Thermal comfort ranking		
		Current	2030s	2050s	Current	2030s	2050s
NS	No overnight setback	3	5	5	11	6	5
ES	Extended morning setback	22	23	23	18	16	16
DS	Delayed evening setback	13	13	13	9	9	9
OMC-H	Occupant manual heating setpoint change	16	16	16	20	20	20
OMC-C	Occupant manual cooling setpoint change	9	10	11	5	5	5
CT-P	Cooling coil SA temperature sensor positive bias	5	4	4	4	4	4
CT-N	Cooling coil SA temperature sensor negative bias	18	18	17	24	24	24
HT-P	Heating coil SA temperature sensor positive bias	14	14	14	6	8	8
HT-N	Heating coil SA temperature sensor negative bias	10	9	8	21	21	21
OAT-P	Economizer OA temperature sensor positive bias	19	19	19	12	12	12
OAT-N	Economizer OA temperature sensor negative bias	21	21	21	15	17	18
RAT-P	Economizer RA temperature sensor positive bias	23	22	22	19	19	19
RAT-N	Economizer RA temperature sensor negative bias	25	25	25	13	13	13
TH-P	Thermostat positive offset	6	6	6	2	2	2
TH-N	Thermostat negative offset	15	15	15	23	23	23
SFD	Supply fan motor efficiency degradation	17	17	18	14	14	14
SFmin	Supply fan stuck at min speed	4	3	3	25	25	25
SF50	Supply fan stuck at 50% speed	12	12	12	3	3	3
SFmax	Supply fan stuck at max speed	1	1	1	1	1	1
OD0	OA damper stuck fully closed	7	7	10	7	7	7
OD50	OA damper stuck 50% position	8	8	7	10	10	10
OD100	OA damper stuck fully open	2	2	2	8	11	11
ODL	OA damper leakage	20	20	20	17	17	17
VRCF	VAV reheat coils complete failure	24	24	24	15	15	15
SDL	Supply air duct leakage	11	11	9	22	22	22

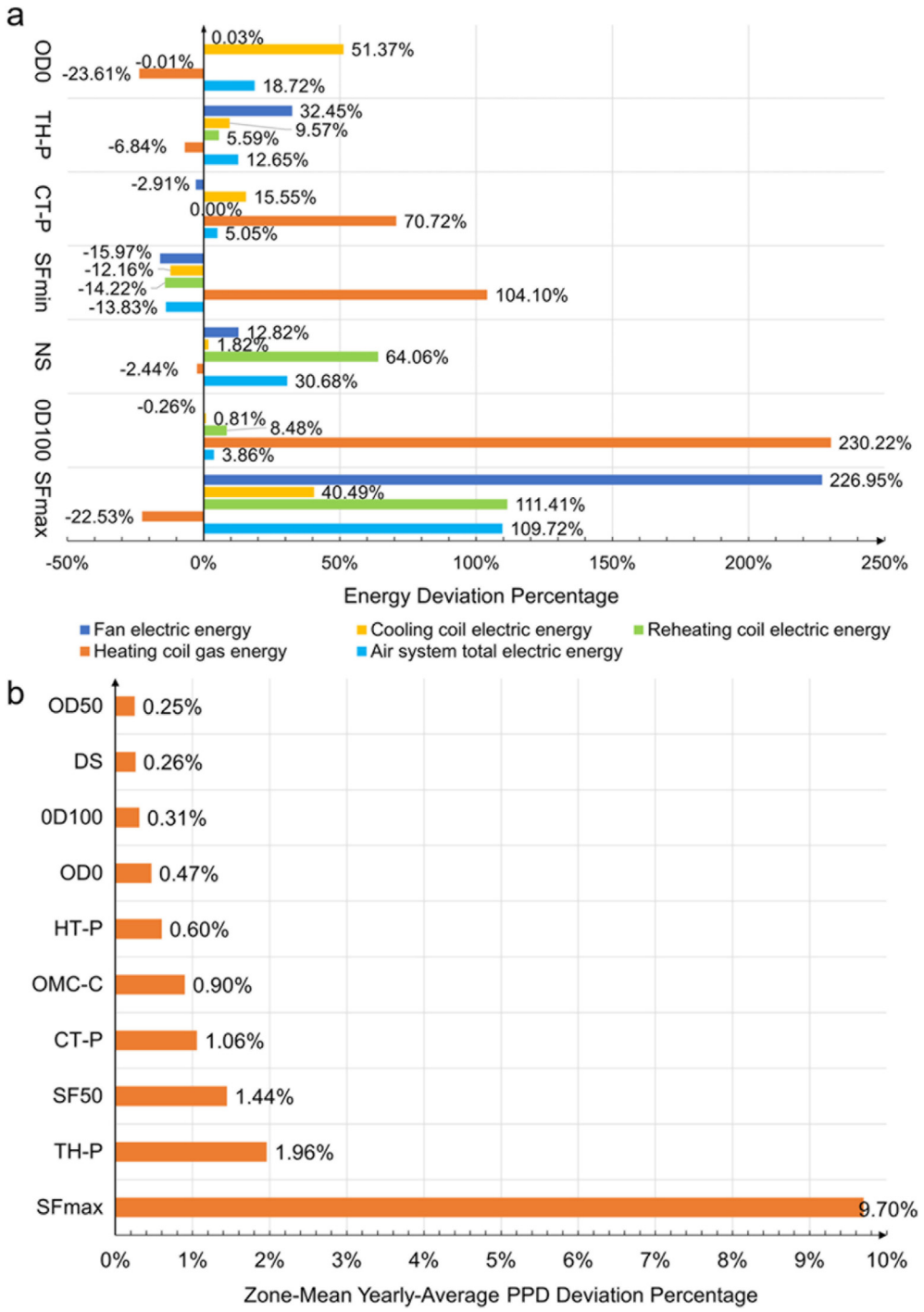

Fig. 4. Single fault impacts under the current climate period: (a) System energy usage deviations; (b) PPD deviations for the top-ranked faults.

of 70.72% (Fig. 4a) since cooling is turned on in the heating season to mitigate the overheating effect on zones (Fig. 6d).

As for thermostat positive offset, it showed a substantial effect on occupant thermal comfort (Fig. 4b). The main reason for the effect is that the thermostat reading reached the zone air temperature setpoint when the actual zone air temperature was lower than the setpoint. As a result, the temperature of SA leaving the heating coil during the heating season (Fig. 6e) and that leaving the cooling coil during the cooling season (Fig. 6f) were both lower than the actual required SA temperature, which led to the decrease in heating coil gas energy of 6.84% and the increase in cooling coil electric energy of 9.57% (Fig. 4a), respectively. To compensate for the less heating effect of SA from the packaged air conditioner, the SA flow rate was increased in the heating season (Fig. 6e). Moreover, the SA flow rate in the cooling season was also increased (Fig. 6f) to reduce the actual air temperature of the faulty zone to ensure that the positive-deviated reading of the thermostat meets the zone air temperature setpoint.

Under the 2050s period, similar trends in energy end usages for the top 7 faults can still be observed in Fig. 5a. Supply fan stuck at

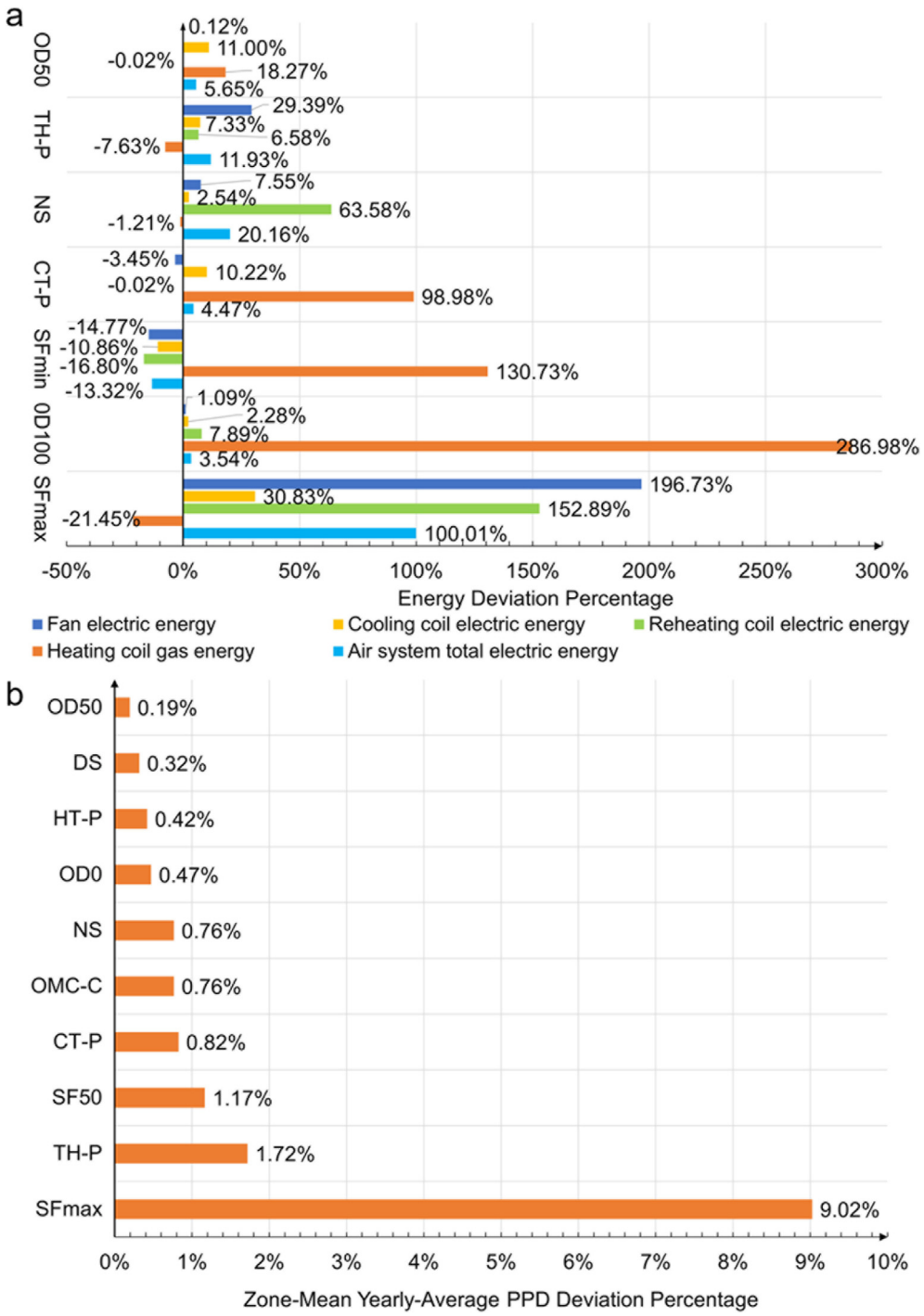

Fig. 5. Single fault impacts under the 2050s climate period: (a) System energy usage deviations; (b) PPD deviations for the top-ranked faults.

maximum speed still resulted in the most significant energy impact (Fig. 5a). Compared with the ranks under the current period, the rank ascending for supply fan stuck at minimum speed and cooling coil SA temperature sensor positive bias, as presented in Table 4, were mainly due to their intensified impacts on heating coil gas energy (Fig. 5a). Apart from these, the rank descending for no overnight setback, as presented in Table 4, was caused by the reduced effect on the fan and reheat coil electric energy (Fig. 5a). As for the only difference among the top 7 faults in the energy impact ranking between the current and 2050s periods, the OA damper stuck at 50% position resulted in large deviations in heating coil gas energy and cooling coil electric energy from the baseline normal case (Fig. 5a). Regarding the PPD for the top 10 faults, the most significant impact of 9.02% was also led by supply fan stuck at maximum speed (Fig. 5b). The deviations of system energy end usages and PPD from the baseline normal case under the 2030s period can be found in Fig. A1 in Appendix A.

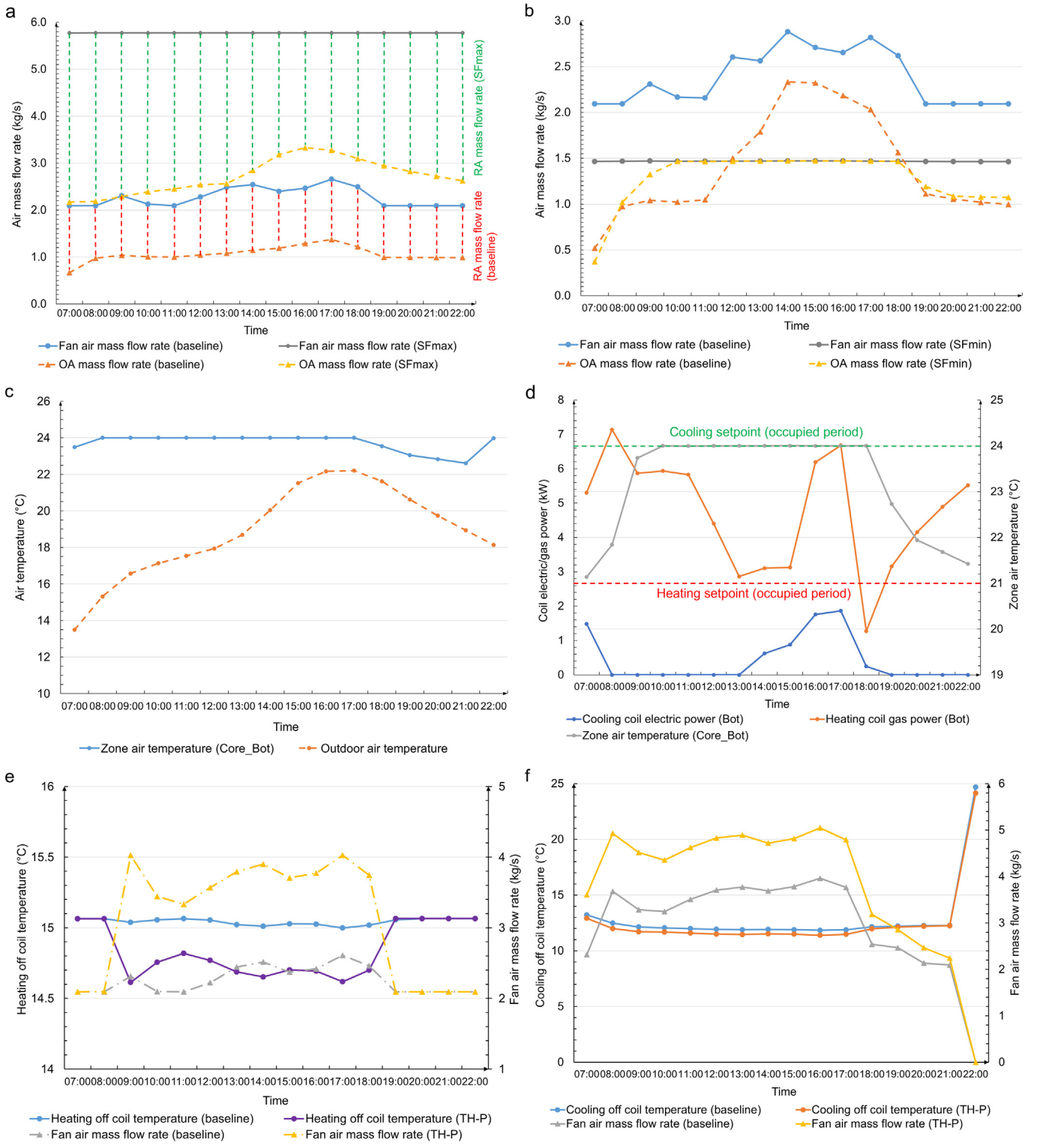

Fig. 6. Causes for the impacts of single faults: (a) Supply fan stuck at maximum speed; (b) Supply fan stuck at minimum speed; (c) No overnight setback and OA damper stuck fully closed; (d) Cooling coil SA temperature sensor positive bias; (e–f) Thermostat positive offset.

4.2. Multiple fault impact and rankings

A general overview of the rankings for each multiple faults combination, in terms of energy and thermal comfort impact, are listed in Table 5. Each fault combination is ranked based on the proposed energy and thermal comfort indicators from Eqns. (2) and (3) under the current, 2030s and 2050s periods. The differences between the actual combined effects and the algebraic sums were found to be within two categories: synergetic effect and antagonistic effect, which are discussed in subsections 4.2.1 and 4.2.2. Based on Table 5, most multiple faults combinations remain in the same ranks across climate periods. The types of the top 5

Table 5
Energy and thermal comfort impact rankings for multiple faults under each climate period.

Fault type	Energy ranking			Thermal comfort ranking		
	Current	2030s	2050s	Current	2030s	2050s
No overnight setback + Cooling coil SA temperature sensor positive bias	9	9	9	12	10	10
No overnight setback + Supply fan stuck at min speed	15	16	15	15	15	15
No overnight setback + Supply fan stuck at max speed	3	3	3	5	5	4
No overnight setback + OA damper stuck fully closed	14	17	17	13	12	11
No overnight setback + OA damper stuck fully open	5	5	5	14	14	13
Cooling coil SA temperature sensor positive bias + Supply fan stuck at min speed	17	15	13	16	17	17
Cooling coil SA temperature sensor positive bias + Supply fan stuck at max speed	2	2	2	1	1	1
Cooling coil SA temperature sensor positive bias + OA damper stuck fully closed	13	12	12	10	11	12
Cooling coil SA temperature sensor positive bias + OA damper stuck fully open	8	8	8	11	13	14
Supply fan stuck at min speed + OA damper stuck fully closed	19	19	19	17	18	18
Supply fan stuck at min speed + OA damper stuck fully open	12	10	10	18	19	19
Supply fan stuck at max speed + OA damper stuck fully closed	4	4	4	3	3	2
Supply fan stuck at max speed + OA damper stuck fully open	1	1	1	2	2	5
No overnight setback + Thermostat positive offset	11	14	16	6	6	6
Cooling coil supply air temperature sensor positive bias + Thermostat positive offset	10	11	11	7	7	7
Thermostat positive offset + Supply fan stuck at min speed	16	13	14	19	16	16
Thermostat positive offset + Supply fan stuck at max speed	6	6	6	4	4	3
Thermostat positive offset + OA damper stuck fully closed	18	18	18	8	8	8
Thermostat positive offset + OA damper stuck fully open	7	7	7	9	9	9

combinations in both energy and thermal comfort rankings keep the same, but the ranks of the top 5 combinations in terms of thermal comfort vary significantly from the current and 2030s periods to 2050s period.

4.2.1. Multiple faults synergetic effect

The differences between actual combined effects and algebraic sums, in terms of system energy usages and occupant thermal comfort, for the top 5 combinations under the current period from Table 5 are illustrated in Fig. 7a and b, respectively. The synergetic effect, which means that the actual combined effect is larger than the algebraic sum, is indicated in system energy usages of the top 5 combinations. Under the current period, some cases demonstrate that the actual combined effects on energy usages are significantly higher than the algebraic sums. The combination of cooling coil SA temperature sensor positive bias and supply fan stuck at maximum speed showed an enormous increase of 135.17% from the algebraic sum in heating coil gas energy (Fig. 7a). It should be noted that the two single faults led to an increase of 70.72% and a decrease of 22.53% in heating coil gas energy (Fig. 4a), respectively. One of the main reasons for this phenomenon is that cooling coil SA temperature sensor positive bias caused SA temperature difference of 1 °C to 2 °C across the heating coil (Fig. 8a), which was zero when only supply fan stuck at maximum speed occurred since the large portion of RA in the mixed air offsets the need for heating the supply air. Another reason is that the SA flow rate was increased considerably (Fig. 8a) due to the maximum operating speed of the supply fan.

Similarly, substantial increases of +90.47% and +68.51% from the algebraic sum in heating coil gas energy were led by the combinations of no overnight setback and OA damper stuck fully open, and supply fan stuck at maximum speed and OA damper stuck fully open (Fig. 7a). Although no overnight setback and supply fan stuck at maximum speed individually resulted in decreases in heating coil gas energy (Fig. 4a), the SA temperature difference across the heating coil was increased substantially (Fig. 8b–c) when OA damper stuck fully open occurred. As a result, the actual combined effects of these combinations on heating coil gas energy were considerable.

Apart from the large increase from the algebraic sum in heating coil gas energy, the combination of supply fan stuck at maximum speed and OA damper stuck fully open also resulted in a significant increase of 82.26% from the algebraic sum in reheating coil electric energy (Fig. 7a). The large deviation can be attributed to the significantly increased zone SA temperature difference across reheating coils caused by both faults and the considerably increased zone SA flow rate due to the increased SA flow rate from the packaged air conditioner (Fig. 8d).

With respect to electricity consumed by cooling coils, a large increase of 22.82% from the algebraic sum in cooling coil electricity usage was caused by the combination of cooling coil SA temperature sensor positive bias and supply fan stuck at maximum speed (Fig. 7a). This increase was due to the increased SA flow rate caused by the supply fan stuck at maximum speed and the increased SA temperature difference across the cooling coil led by the cooling coil SA temperature sensor positive bias (Fig. 8e).

Based on variations in the synergetic effects for system energy usages across the climate periods, as presented in Fig. 9a–e, the synergetic effect on heating coil gas energy and reheating coil electric energy for several fault combinations is intensified with the transition from the current to the 2050s period. The most significant increase from the algebraic sum in heating coil gas energy was caused by the combination of cooling coil SA temperature sensor positive bias and supply fan stuck at maximum speed, which increased from 135.17% to 163.67% (Fig. 9b). In addition, the increase from the algebraic sum in reheating coil electric energy for the combination of supply fan stuck at maximum speed and outdoor air damper stuck fully open was intensified across the climate periods from 82.26% to 105.97% (Fig. 9c). On the other hand, the synergetic effects on the air system total, cooling coil and fan electric energy are reduced across the climate periods (Fig. 9a, d, e). As for the synergetic effect on thermal comfort, the variation from the algebraic sum in the PPD for the combination of cooling coil SA temperature sensor positive bias and supply fan stuck at maximum speed increased from +1.84% under the current period to +2.07% under 2030s period, and then decreased to +1.86% under 2050s period (Fig. 9f). The comparisons between actual combined effects of the top 5 fault combinations, and the algebraic sums of each single-fault impact involved in each combination under the 2030s and 2050s periods can be found in Figs. A2 and A3, respectively, in the Appendix A.

4.2.2. Multiple faults antagonistic effect

The differences between actual combined effects and algebraic

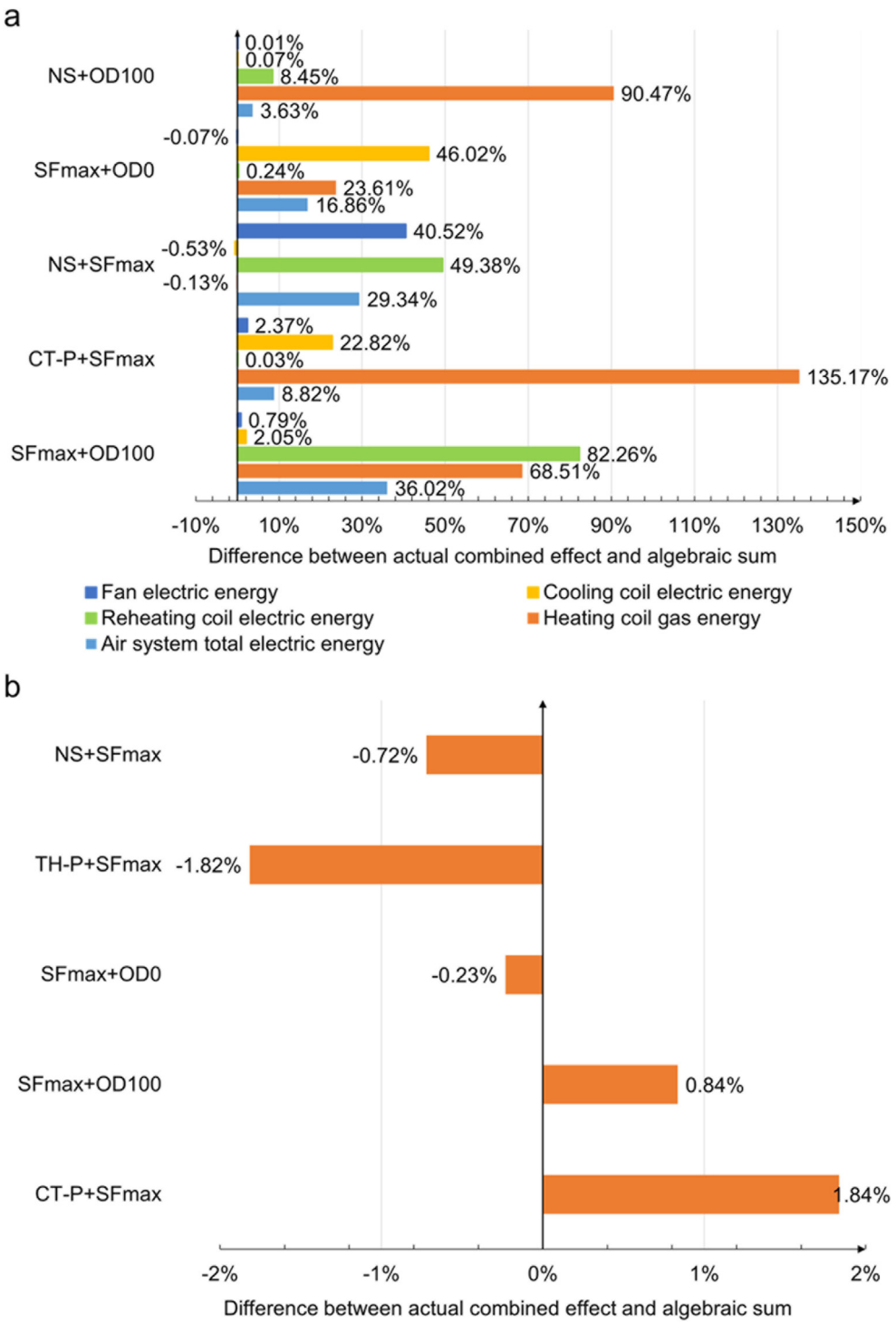

Fig. 7. Multiple faults interactions for the top 5 combinations under the current climate period: (a) Differences between the actual combined effects on (a) system energy consumptions; (b) PPD, and the algebraic sums of each single-fault impact.

sums, in terms of system energy usages, for the fault combinations with severe antagonistic effects under the current period from Table 5 are shown in Fig. 10. In contrast to the synergetic effect, the antagonistic effect, which represents a less actual combined effect than the algebraic sum, is also presented in energy end usages of some multiple faults combinations. Under the current period, the combinations of supply fan stuck at minimum speed with OA damper stuck fully closed, and with OA damper stuck fully open indicated substantial decreases of 104.45% and 166.97% from the algebraic sums in heating coil gas energy, respectively (Fig. 10). The supply fan stuck at minimum speed and OA damper stuck fully open individually caused significant increases in heating coil gas energy of 104.10% and 230.22% (Fig. 4a), while OA damper stuck fully closed individually led to a decrease in heating coil gas energy of 23.61% (Fig. 4a). A common reason for them was that the minimum operation speed of the supply fan limited OA's intake, thus

Fig. 8. Causes for multiple faults: (a–e) synergetic effects and (f–h) antagonistic effects.

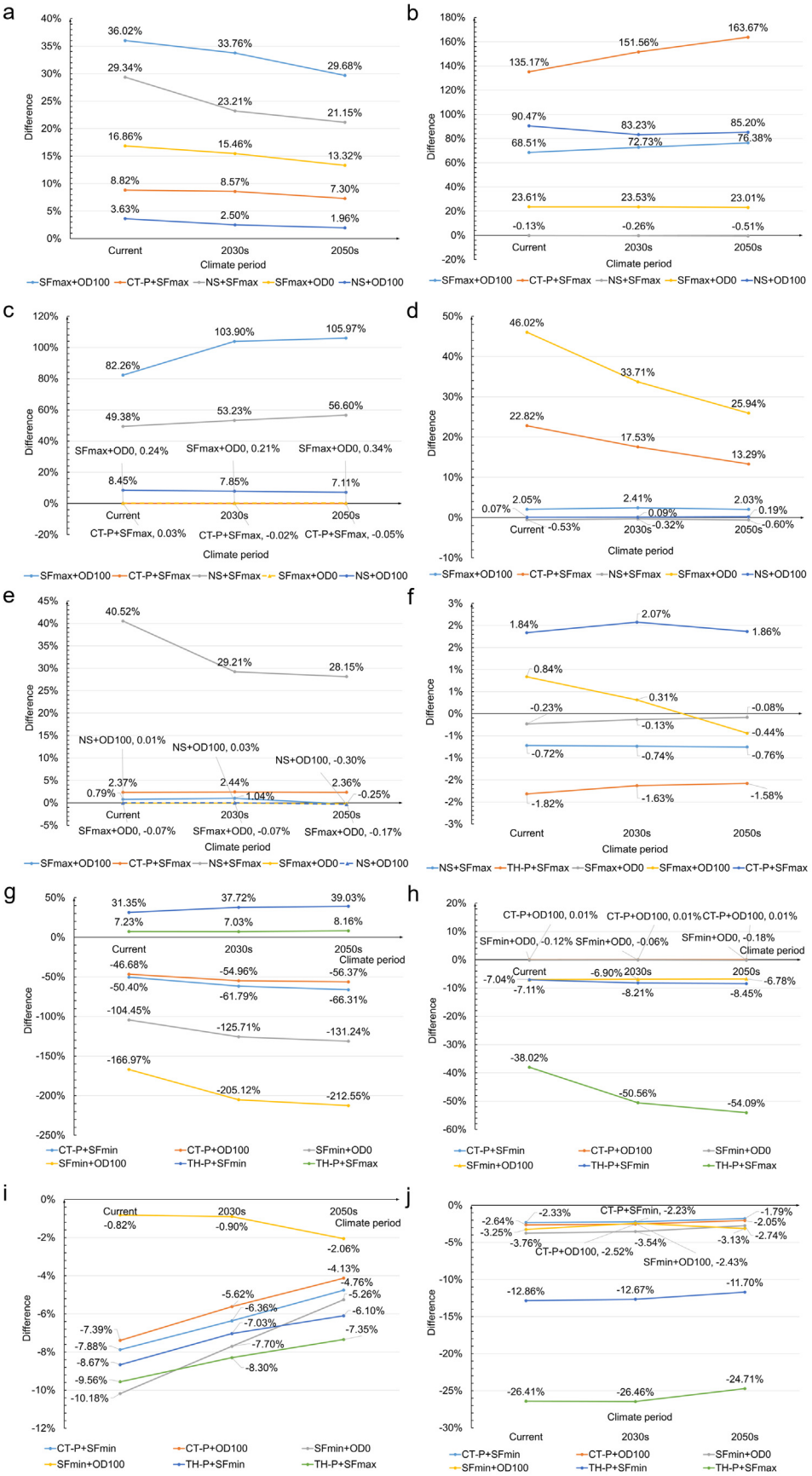

Fig. 9. Variations across climate periods in the differences between actual combined effects and algebraic sums (known as 'Difference' in the figures) of (a) air system total electric energy; (b) heating coil gas energy; (c) reheating coil electric energy; (d) cooling coil electric energy; (e) fan electric energy; (f) PPD for the top 5 fault combinations; (g) heating coil gas energy (h) reheating coil electric energy; (i) cooling coil electric energy; (j) air system total electric energy for the fault combinations with severe antagonistic effects.

reducing the need for heating the mixed air (Fig. 8f–g). In addition, the fully closed OA damper led to the full RA ratio for the mixed air, therefore minimising the SA temperature difference across the heating coil to zero (Fig. 8f).

As for the antagonistic effects on other system energy end usages, the largest decrease of 38.02% from the algebraic sum in reheating coil electric energy was caused by the combination of thermostat positive offset and supply fan stuck at maximum speed (Fig. 10). As shown in Fig. 8h, the supply fan stuck at maximum speed induced large SA temperature differences across the reheat coil, but thermostat positive offset minimised the need for reheating the supply air to zero and thus led to this large decrease.

The variations in the antagonistic effects on system energy usages across the climate periods for these combinations are plotted in Fig. 9g–j. The most remarkable effects are still presented on heating coil gas energy for several fault combinations. The largest decrease of 212.55% from the algebraic sum (Fig. 9g) was triggered by the combination of supply fan stuck at minimum speed and OA damper stuck fully open under the 2050s period, which was intensified from 166.97% under the current period (Fig. 9g). In contrast, the deviations from the algebraic sums in cooling coil electric energy for all the fault combinations, except the combination of supply fan stuck at minimum speed and OA damper stuck fully open, were mitigated across the climate periods (Fig. 9i). Moreover, considerable enhancement in the antagonistic effect on reheating coil electric energy was indicated by the combination of thermostat positive offset and supply fan stuck at maximum speed with decreases from 38.02% to 54.09% (Fig. 9h). Regarding the air system's total electric energy, it can be obviously observed that the variations in the antagonistic effects for all the fault combinations are insignificant (Fig. 9j). Apart from these, an obvious difference among the climate periods is that the synergetic effect on PPD for the combination of supply fan stuck at max speed and OA damper stuck fully open decreased from +0.84% under current period to +0.31% under 2030s period, and further being converted to the antagonistic effect of −0.44% under 2050s period (Fig. 9f). The comparisons between actual combined effects of the fault combinations with severe antagonistic effects, and the algebraic sums of each single-fault impact involved in each combination under the 2030s and 2050s periods can be found in Figs. A4 and A5, respectively, in the Appendix A.

4.3. Fault impact variations driven by climate change

This section provides the variations of single and multiple faults impacts on system energy end usages and occupant thermal comfort from the current to the 2030s period and from the current to the 2050s period, respectively.

4.3.1. Single fault impact variations

The variations of energy end usages and the PPD for each single fault between the 2030s and current periods and between the 2050s and current periods are presented in Fig. 11. Overall, the cooling coil and fan electric energy for all single faults increased by the ranges of 29.5–35.5 GJ (Fig. 11b) and 5.4–9.6 GJ (Fig. 11e), respectively, from the current to 2030s period and grown by the ranges of 56.3–72.0 GJ (Fig. 11b) and 6.9–11.5 GJ (Fig. 11e), respectively, from the current to 2050s period. In contrast, the heating coil gas energy and reheating coils electric energy for all single faults reduced by the ranges of 8.5–13.7 GJ (Fig. 11c) and 33.0–61.5 GJ (Fig. 11d), respectively, from the current to 2030s period and decreased by the ranges of 11.1–24.0 GJ (Fig. 11c) and 38.6–69.6 GJ (Fig. 11d), respectively, from the current to 2050s period.

Apart from these, most single faults increased by around

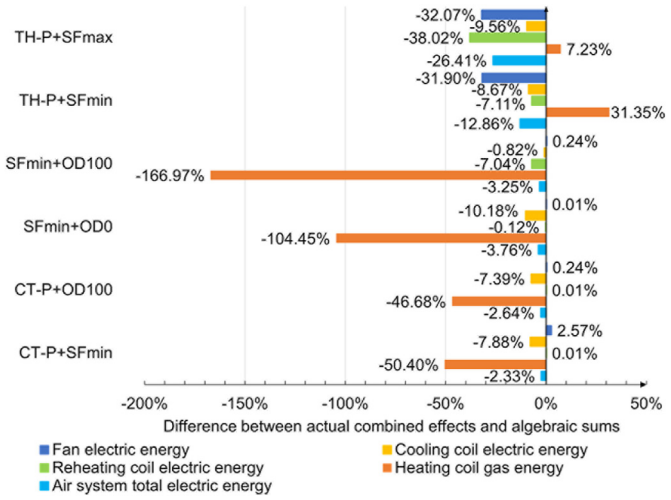

Fig. 10. The antagonistic effects of multiple faults combinations on system energy consumptions under the current climate period.

2.0–7.0 GJ in air system total electric energy from the current to 2030s period (Fig. 11a). Regarding the variations from the current to 2050s period, the air system total electric energy increased dramatically by 20.2–32.5 GJ compared with the 2030s period. The largest increase in air system total electric energy of 34.3 GJ was caused by heating coil SA temperature sensor negative bias from the current to 2050s period (Fig. 11a). In terms of thermal comfort, the PPDs for all single faults decreased by 2.2%–3.6% from the current to 2030s period and reduced by 2.3%–4.0% from the current to 2050s period (Fig. 11f). The increasing OA temperature in winter can explain these trends as the occupant thermal discomfort mainly originates from the heating season (Fig. 11g–h).

4.3.2. Multiple fault combinations impact variations

The variations in energy end usages and the PPD for each fault combination from the current to 2030s and from the current to 2050s are illustrated in Fig. 12. In contrast to the small increases and even significant decreases in air system total electric energy between the current and 2030s periods, the variations in air system total electric energy for most fault combinations increased substantially under the 2050s period (Fig. 12a). The most increase from the current period was boosted from 5.1 GJ by the combination of thermostat positive offset and supply fan stuck at minimum speed under the 2030s period to 35.3 GJ by the combination of thermostat positive offset and outdoor air damper stuck fully open under the 2050s period (Fig. 12a).

Additionally, the approximately double increases of 53.4 GJ–76.5 GJ in cooling coil electric energy between the current and 2050s periods, compared with those of 29.3 GJ–37.2 GJ between the current and 2030s periods (Fig. 12b), are responsible for the significant increases in air system total electric energy under the 2050s period. Apart from these, the heating coil gas energy and reheating coil electric energy decreased by 7.5 GJ–26.8 GJ and 32.8 GJ–82.2 GJ, respectively, from the current to 2030s period and reduced by 9.8 GJ–39.0 GJ and 38.3 GJ–90.3 GJ, respectively from the current to 2050s period (Fig. 12c–d). Moreover, the fault combinations, except no overnight setback and supply fan stuck at maximum speed, resulted in increases in fan electric energy by the range of 4.9–9.4 GJ from the current to 2030s period and 6.3–12.2 GJ from the current to 2050s period (Fig. 12e). With respect to thermal comfort, the PPDs for fault combinations reduced by the ranges of 1.9%–4.3% from the current to 2030s

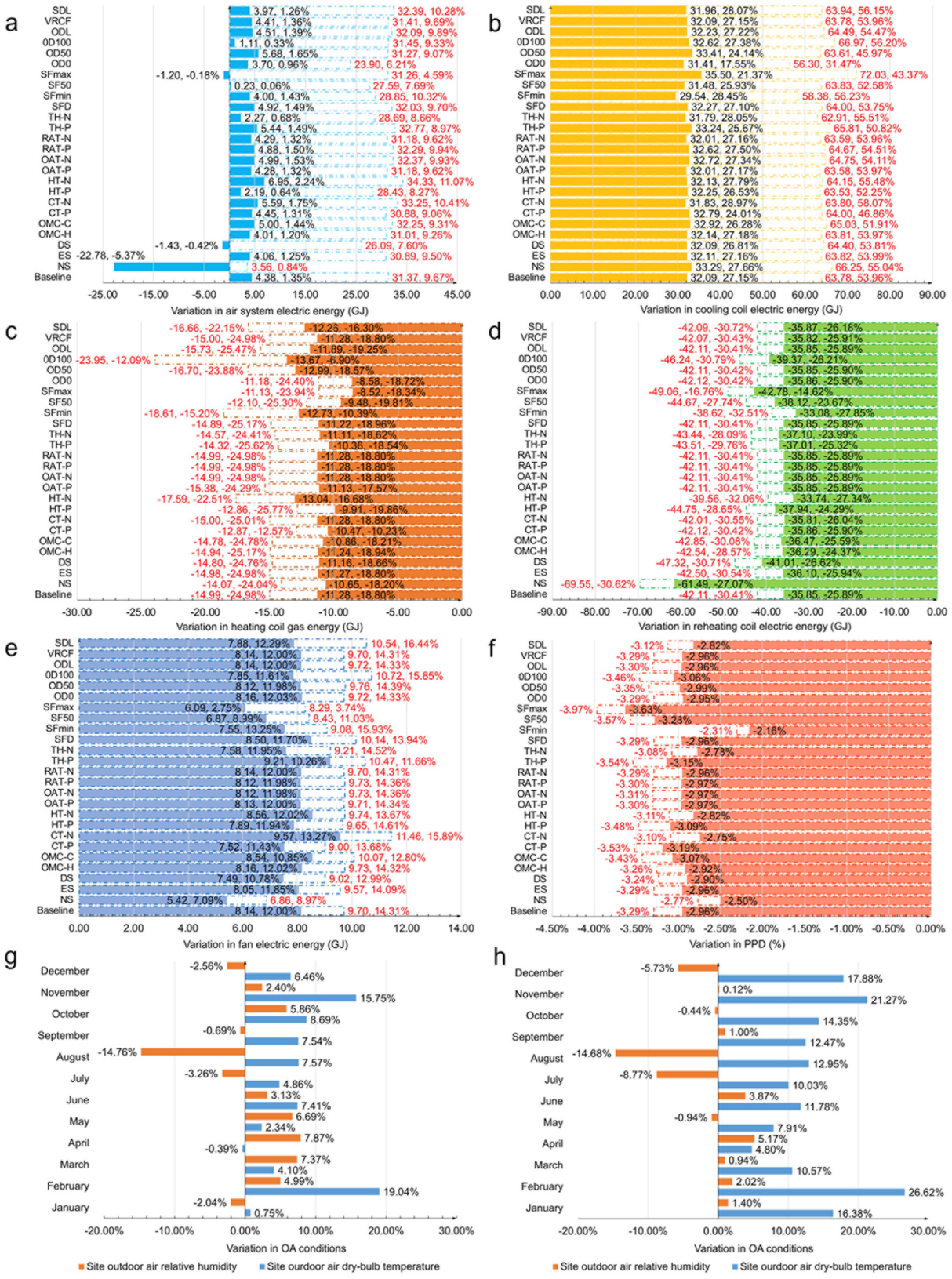

Fig. 11. (a–f) Variations in air system total electric energy, cooling coil electric energy, heating coil gas energy, reheating coil electric energy, fan electric energy and PPD for single faults from the current to the 2030s period (in solid fill & black labels) and from the current to the 2050s period (in dash-dot line & red labels). (First label for each bar: the variation amount, second label: the variation percentage); Variations in OA dry-bulb temperature and relative humidity between (g) the current and 2030s periods; (h) the current and 2050s periods.

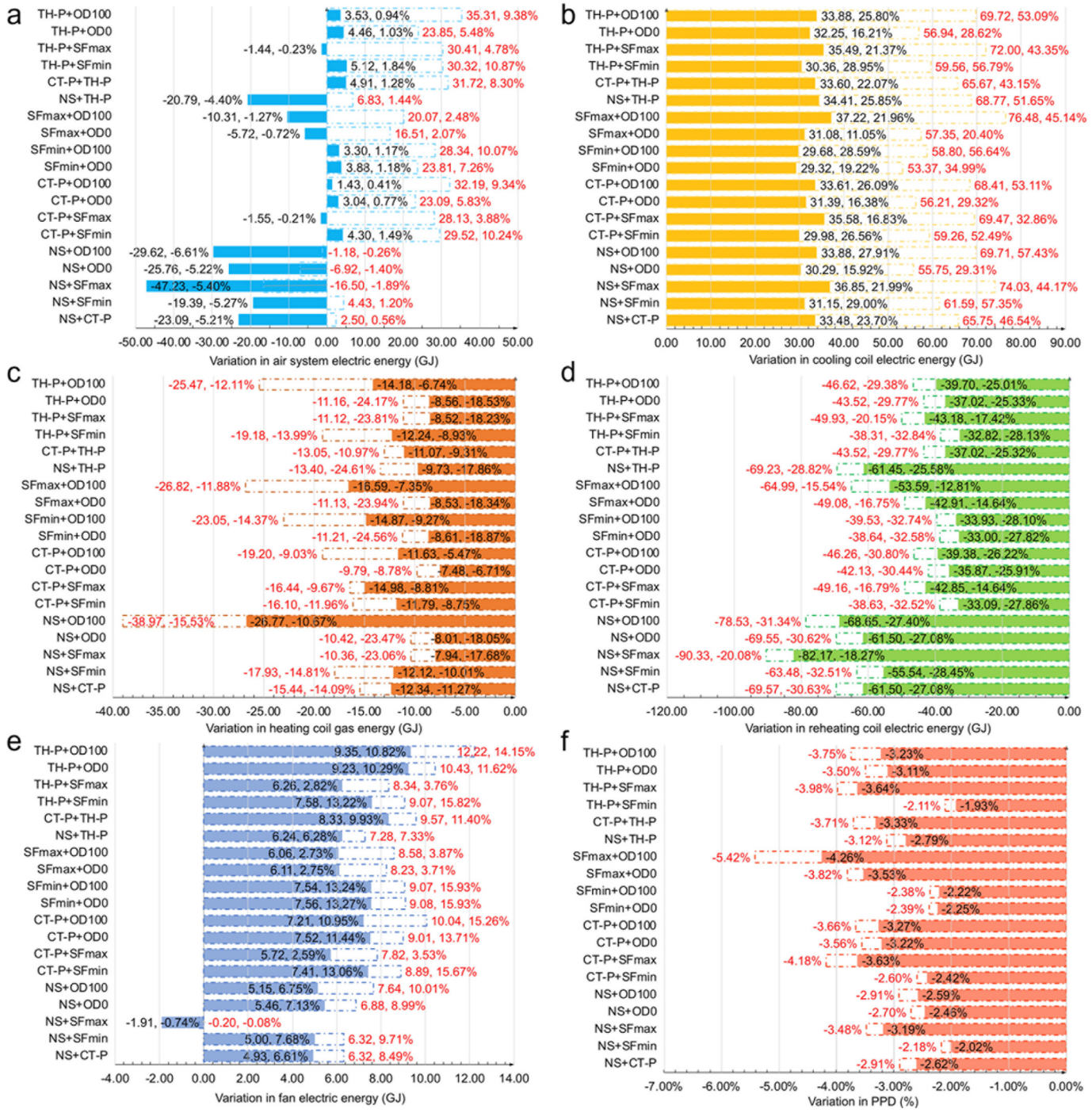

Fig. 12. (a–f) Variations in air system total electric energy, cooling coil electric energy, heating coil gas energy, reheating coil electric energy, fan electric energy and PPD for multiple faults combinations from the current period to the 2030s period (in solid fill & black labels) and from the current period to the 2050s period (in dash-dot line & red labels). (First label for each bar: the variation amount, second label: the variation percentage).

period and 2.1%–5.4% from the current to 2050s period (Fig. 12f).

4.4. Comparisons with findings from previous studies

The findings from the results of this study are compared with those from previous studies and discussed in terms of three aspects: (1) single fault impacts; (2) multiple faults interactions; (3) HVAC system performance variations driven by climate change.

From the perspective of single fault impacts, Lu et al. [24] also implemented a comprehensive evaluation of fault impacts using the Modelica simulations and highlighted that no overnight setback is one of the faults among the top faults in the energy impact ranking under the current period, which conforms with the finding of this study that this fault is ranked third in terms of energy impact. In addition, OA damper stuck and thermostat positive bias were found to be within the top faults in the thermal comfort impact ranking, which are also verified in this study.

In terms of multiple faults interactions, Zhou et al. [33] and Hu

et al. [34] investigated the interactions among multiple common faults from a different HVAC system to that in this study, variable refrigerant flow system and heat pump system, respectively. Both studies indicated that the impact of multiple faults on the system performances, in terms of cooling capacity and COP, is not an algebraic summation of the impact of each single fault. The impact of each fault can be intensified or cancelled when these faults occur simultaneously, which corresponds to the proposed synergetic and antagonistic effects for multiple faults in the present paper. In this study, the summation rule is also found to be not applicable for the fault impacts of a VAV system and the synergetic and antagonistic effects among multiple faults are verified. However, there is a unique finding proposed in this study, i.e., the synergetic effect of multiple faults can lead to a significantly increased combined fault impact in the case that one fault causes a decrease in an energy end usage and another fault induces an increase in the same energy end usage, and similarly, the antagonistic effect can result in a substantially decreased combined fault impact in the same case.

As for the fault impact variations driven by climate change, due to the lack of studies exploring this, the general trends of fault impact variations across different climate periods are compared with the trends in HVAC system performance variations under normal conditions. Waddicor et al. [53] indicated that the decrease in system heating energy was higher than the increase in system cooling energy from 2020 to 2050 under the climate of Turin. In addition, Kharseh et al. [54] pointed out the same phenomenon from the current to 2050s climate period under the cold climate of Stockholm. The results of this study show a similar trend in fault impact variations from the current to 2030s climate period under the marine climate of London, but demonstrated a reverse trend for most single faults and almost half of multiple faults combinations from the current to 2050s climate period.

5. Conclusion and future works

In this study, the impacts of single and multiple faults from VAV systems on system energy consumptions and occupant thermal comfort were evaluated using the current and future (2030s and 2050s) weather conditions. Based on the fault impact variations from the baseline normal case, the energy and thermal comfort indicators were proposed to rank the single and multiple faults in terms of system energy usages and occupant thermal comfort under each climate period. In addition, the synergetic and antagonistic effect of multiple faults were evaluated, and the causes for these effects were discussed. Moreover, the fault impact variations across climate periods were assessed, and the single and multiple faults with substantial variations were highlighted. The main findings of this study are as follows:

(1) Supply fan stuck at maximum speed led to the most significant impacts on both system energy usages and occupant thermal comfort. In addition, the combinations of this fault with OA damper stuck fully open, and this fault with cooling coil SA temperature sensor positive bias were ranked first in the energy and thermal comfort impact ranking, respectively.
(2) The synergetic effect of multiple faults can lead to a significantly increased combined fault impact in the case that one fault causes a decrease in an energy end usage and another fault induces an increase in the same energy end usage. Similarly, the antagonistic effect can result in a substantially decreased combined fault impact in the same case.
(3) Climate change can have a significant influence on the synergetic and antagonistic effects. The increase from the algebraic sum in heating coil gas energy for the combination of cooling coil SA temperature sensor positive bias and supply fan stuck at maximum speed was intensified from 135.17% under the current period to 163.67% under the 2050s period. On the other hand, the largest decrease from the algebraic sum in the same energy usage for the combination of supply fan stuck at minimum speed and OA damper stuck fully open was also intensified from 166.97% under the current period to 212.55% under the 2050s period.
(4) Under the marine climate, the decrease in system total heating energy is higher than the increase in system cooling energy from the current to 2030s period for all single and multiple faults. However, the increase in system cooling energy exceeds the decrease in system total heating energy from the current to 2050s period for most single faults and almost half of multiple faults combinations.
(5) Heating coil supply air temperature sensor negative bias, and the combination of thermostat positive offset and OA damper stuck fully open led to the most increase in air system total electric energy by 34.3 GJ and 35.3 GJ from the current to 2050s period.

The results of this study are useful for FDD researchers to not only prioritise the FDD for faults with significant impacts, but also pay attention to faults with substantial variations across climate periods, in order to ensure that the FDD framework can adapt to the changes in prioritised faults caused by climate change. In addition, according to the variations in fault impact patterns across climate periods, it is worth highlighting that data-driven FDD methods are required to be updated timely using the latest fault measurements from real buildings or fault data simulated by well-calibrated building models.

The future work can explore the fault impacts under different climate zones, such as hot climates, to compare the differences in fault impacts under different climate zones. In addition, the fault impacts from other types of HVAC systems, such as fan coil systems, are worth to be studied. Besides, the impacts of faults related to the refrigerant cycle of HVAC systems can be further evaluated, and other system performance metrics, such as COP, can be introduced. Moreover, the occurrence frequency of each fault can be taken into account to quantify the fault impacts in a more realistic way if general occurrence frequency data is available. Furthermore, further validation of the building energy modeling should be carried out, in particular on the short-term and dynamic behaviours of the HVAC system.

Declaration of competing interest

The authors declare that they have no known competing financial interests or personal relationships that could have appeared to influence the work reported in this paper.

Data availability

The authors are unable or have chosen not to specify which data has been used.

Appendix A

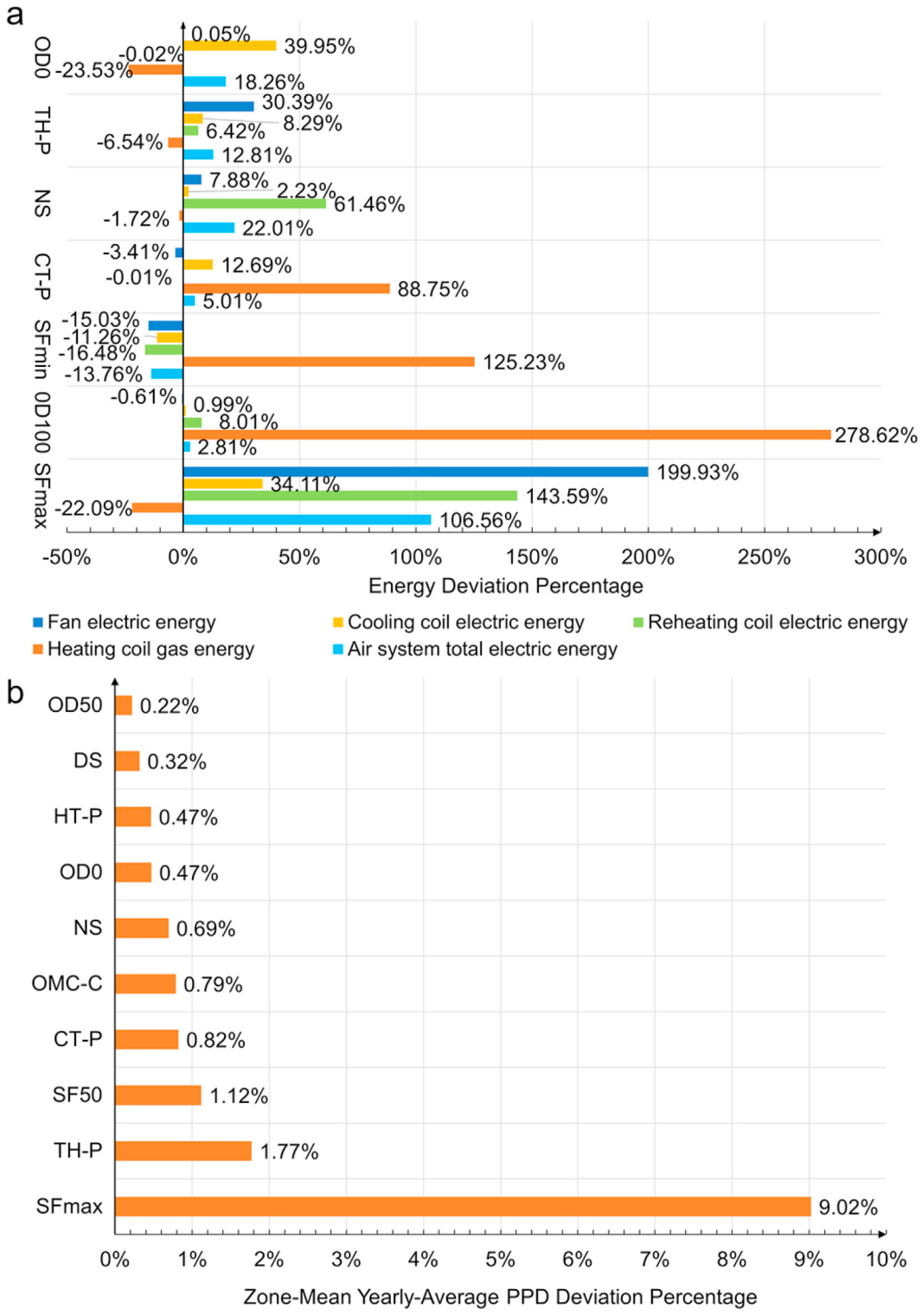

Fig. A1. Single fault impacts under the 2030s climate conditions: (a) System energy usage deviations; (b) PPD deviations for the top-ranked faults.

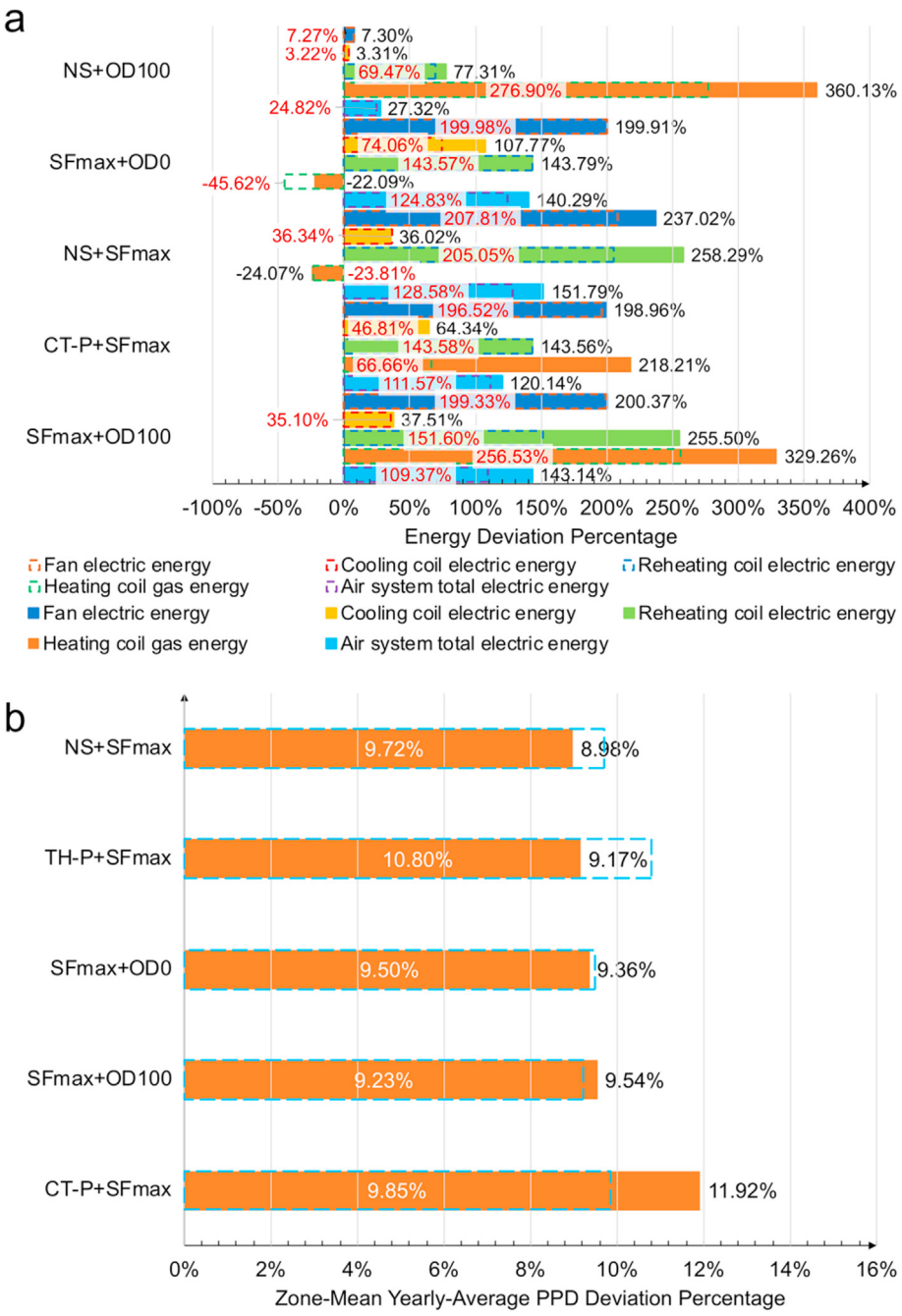

Fig. A2. Multiple faults interactions under the 2030s climate period: Comparison of the actual combined effects on (a) system energy end usages variations; (b) PPD variations and the algebraic sums of the single fault impact variations for the top 5 combinations (solid fill & black labels: actual combined effect; dash line & (a) red labels; (b) white labels: algebraic sum).

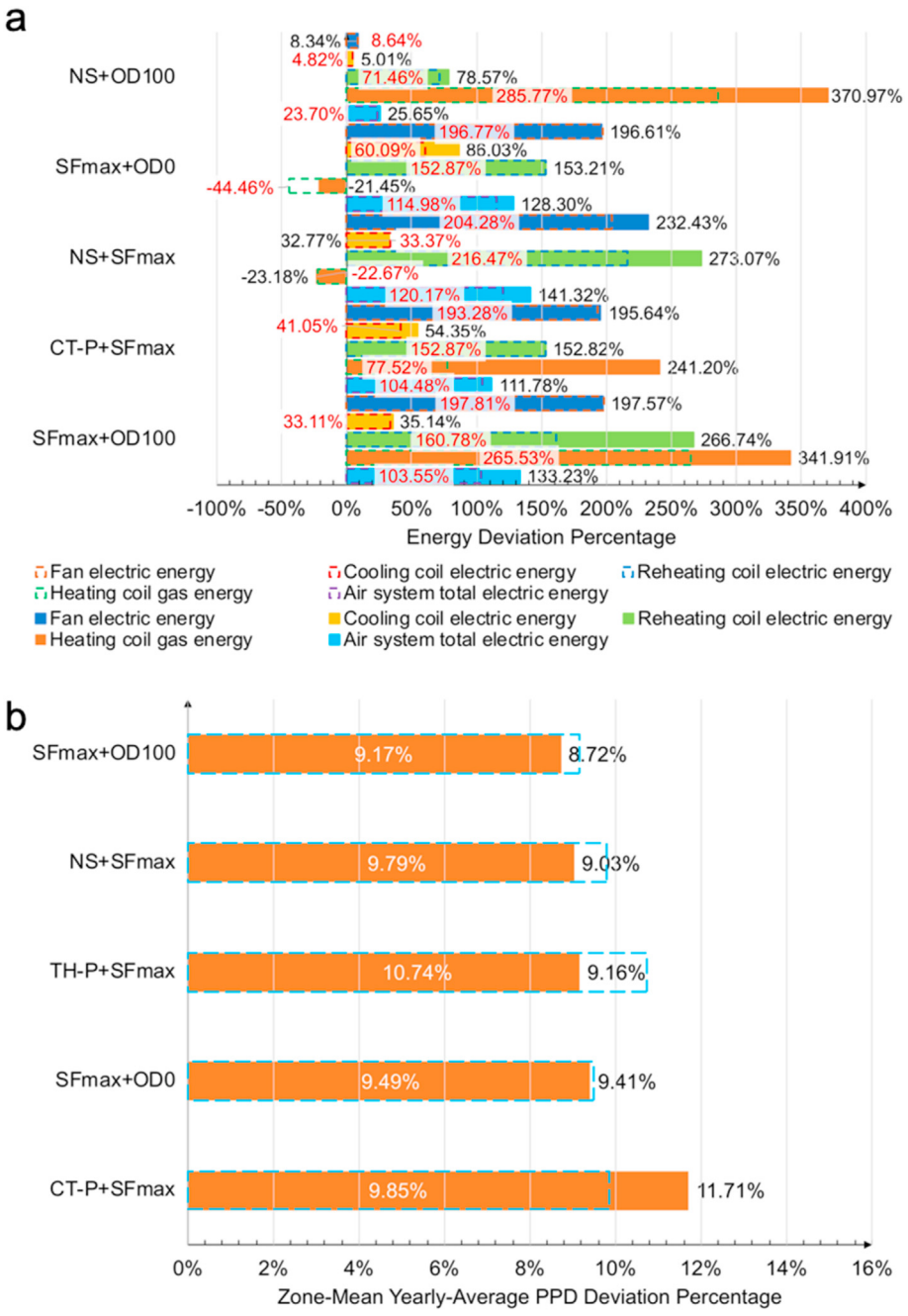

Fig. A3. Multiple faults interactions under the 2050s climate period: Comparison of the actual combined effects on (a) system energy end usages variations; (b) PPD variations and the algebraic sums of the single fault impact variations for the top 5 combinations (solid fill & black labels: actual combined effect; dash line & (a) red labels; (b) white labels: algebraic sum).

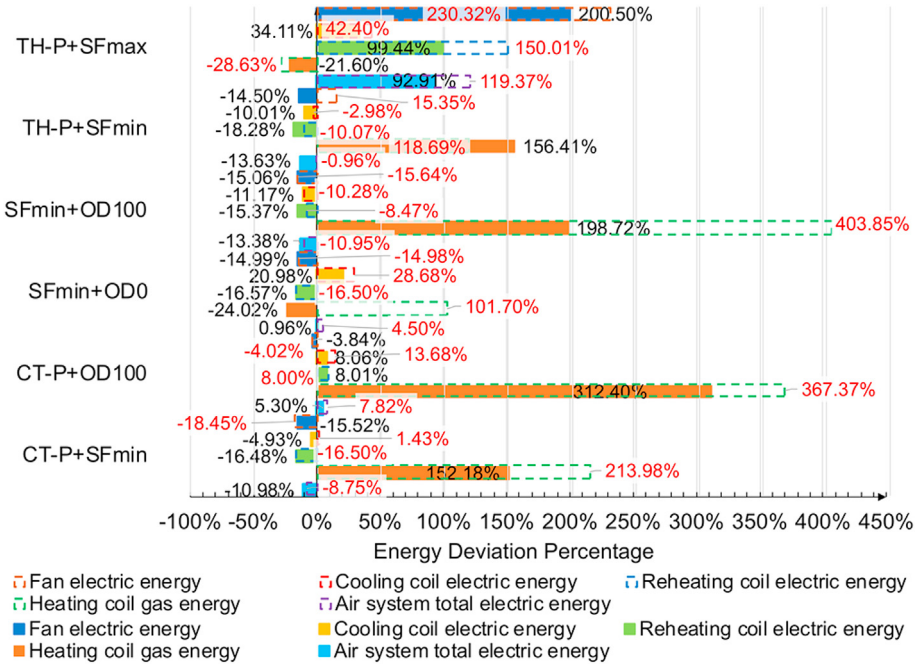

Fig. A4. The antagonistic effects of multiple faults combinations on the deviations of system energy end usages from the baseline normal case under the 2030s climate period (solid fill & black labels: actual combined effect; dash line & red labels: algebraic sum).

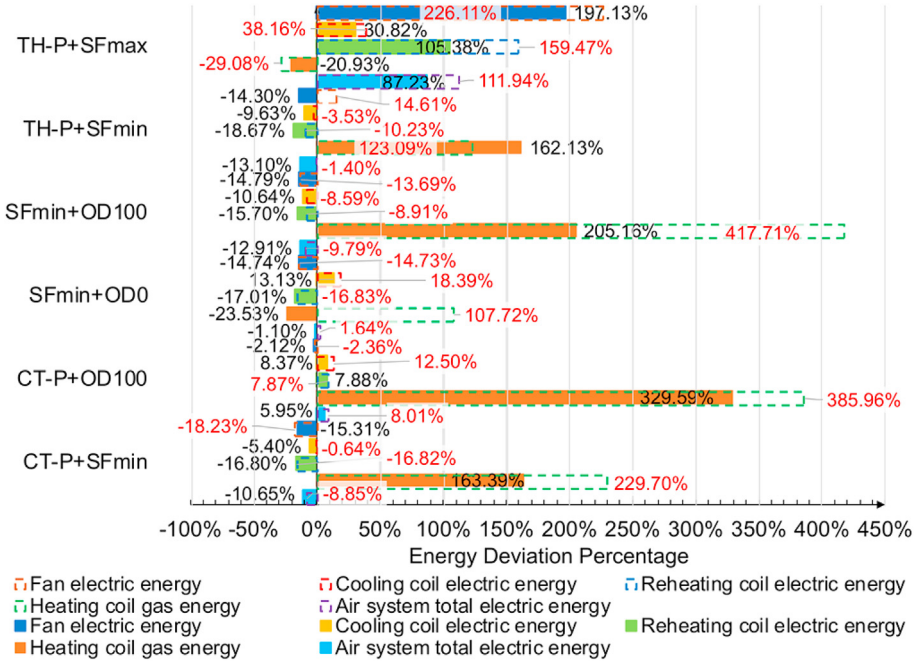

Fig. A5. The antagonistic effects of multiple faults combinations on the deviations of system energy end usages from the baseline normal case under the 2050s climate period (solid fill & black labels: actual combined effect; dash line & red labels: algebraic sum).

Appendix B. Supplementary data

Supplementary data to this article can be found online at https://doi.org/10.1016/j.energy.2022.124762.

References

[1] International Energy Agency (IEA). World energy Outlook 2020. Paris, France: IEA; 2020.
[2] Wu S, Sun J. Cross-level fault detection and diagnosis of building HVAC systems. Build Environ 2011;46(Issue 8):1558–66.
[3] Bahria S, Amirat M, Hamidat A, El-Ganaoui M, Slimani MEA. Parametric study of solar heating and cooling systems in different climates of Algeria - a comparison between conventional and high-energy-performance buildings. Energy 2016;113:521–35.
[4] Carotenuto A, Figaj RD, Vanoli L. A novel solar-geothermal district heating, cooling and domestic hot water system: dynamic simulation and energy-economic analysis. Energy 2017;141:2652–69.
[5] Rana R, Kusy B, Wall J, Hu W. Novel activity classification and occupancy estimation methods for intelligent HVAC (heating, ventilation and air conditioning) systems. Energy 2015;93:245–55.
[6] Turhan C, Simani S, Akkurt GG. Development of a personalized thermal comfort driven controller for HVAC systems. Energy 2021;237:121568.
[7] Downey T, Proctor J. What can 13,000 air conditioners tell us?. In: Proceedings of 2002 American Council for an Energy-Efficient Economy (ACEEE) summer study; 2002. Pacific Grove, August 18-23.
[8] Kim J, Cai J, Braun JE. Common faults and their prioritization in small commercial buildings. Golden, United States: National Renewable Energy Laboratory; 2017.
[9] Schein J, Bushby ST, Castro NS, House JM. A rule-based fault detection method for air handling units. Energy Build 2006;38(Issue 12):1485–92.
[10] Deshmukh S, Samouhos S, Glicksman L, Norford L. Fault detection in commercial building VAV AHU: a case study of an academic building. Energy Build 2019;201:163–73.
[11] Gunay HB, Shi Z, Newsham G, Moromisato R. Detection of zone sensor and actuator faults through inverse greybox modelling. Build Environ 2020;171:106659.
[12] Eom YH, Yoo JW, Hong SB, Kim MS. Refrigerant charge fault detection method of air source heat pump system using convolutional neural network for energy saving. Energy 2019;187:115877.
[13] Wang H, Feng D, Liu K. Fault detection and diagnosis for multiple faults of VAV terminals using self-adaptive model and layered random forest. Build Environ 2021;193:107667.
[14] Li Y, O'Neill Z. A critical review of fault modeling of HVAC systems in buildings. Build Simulat 2018;11:953–75.
[15] Cheung H, Braun JE. Development of fault models for hybrid fault detection and diagnostics algorithm. Golden, United States: National Renewable Energy Laboratory; 2015.
[16] Kim J, Frank S, Braun JE, Goldwasser D. Representing small commercial building faults in EnergyPlus, Part I: model development. Buildings 2019;9(Issue 11). No. 233.
[17] Lu X, O'Neill Z, Li Y, Niu F. A novel simulation-based framework for sensor error impact analysis in smart building systems: a case study for a demand-controlled ventilation system. Appl Energy 2020;263:114638.
[18] U.S. Department of Energy (DOE). EnergyPlus version 9.3 getting started. Washington, D.C., United States: DOE; 2020.
[19] Reddy TA, Maor I, Panjapornpon C. Calibrating detailed building energy simulation programs with measured data— Part I: general methodology (RP-1051). HVAC R Res 2007;13(2):221–41.
[20] The American Society of Heating, Refrigerating and Air-Conditioning Engineers (ASHRAE), *ASHRAE guideline 14-2014, Measurement of energy, demand, and water savings*. Atlanta, United States: ASHRAE; 2014.
[21] Lee SH, Yik FWH. A study on the energy penalty of various air-side system faults in buildings. Energy Build 2010;42(Issue 1):2–10.
[22] Basarkar M, Pang X, Wang L, Haves P, Hong T. Modeling and simulation of HVAC faults in EnergyPlus. In: Proceedings of building simulation 2011: 12th conference of international building performance simulation association. Berkeley, United States: Lawrence Berkeley National Laboratory; 2011. Sydney, Australia, November 14-16, 2011.
[23] Zhang R, Hong T. Modeling of HVAC operational faults in building performance simulation. Appl Energy 2017;202:178–88.
[24] Lu X, Fu Y, O'Neill Z, Wen J. A holistic fault impact analysis of the high-performance sequences of operation for HVAC systems: Modelica-based case study in a medium-office building. Energy Build 2021;252:111448.
[25] Huang S, Zuo W, Vrabie D, Xu R. Modelica-based system modeling for studying control-related faults in chiller plants and boiler plants serving large office buildings. J Build Eng 2021;44:102654.
[26] Cheung H, Braun JE. Empirical modeling of the impacts of faults on water-cooled chiller power consumption for use in building simulation programs. Appl Therm Eng 2016;99:756–64.
[27] Hu Y, Yuill DP. Impacts of common faults on an air conditioner with a microtube condenser and analysis of fault characteristic features. Energy Build 2022;254:111630.
[28] Hu Y, Yuill DP, Ebrahimifakhar A, Rooholghodos A. An experimental study of the behavior of a high efficiency residential heat pump in cooling mode with common installation faults imposed. Appl Therm Eng 2021;184:116116.
[29] Ginestet S, Marchio D, Morisot O. Evaluation of faults impacts on energy consumption and indoor air quality on an air handling unit. Energy Build 2008;40(Issue 1):51–7.
[30] Wang L, Hong T. Modeling and simulation of HVAC faulty operations and performance degradation due to maintenance issues. In: Proceedings of 1st Asia conference of international building performance simulation association; 2012. Shanghai, China, November 25-27.
[31] Li Y, O'Neill Z. An innovative fault impact analysis framework for enhancing building operations. Energy Build 2019;199:311–31.
[32] Yoon S, Yu Y, Wang J, Wang P. Impacts of HVACR temperature sensor offsets on building energy performance and occupant thermal comfort. Build Simulat 2019;12:259–71.
[33] Zhou Z, Chen H, Xing L, Li G, Gou W. An experimental study of the behavior of a model variable refrigerant flow system with common faults. Appl Therm Eng 2022;202:117852.
[34] Hu Y, Yuill DP, Rooholghodos SA, Ebrahimifakhar A, Chen Y. Impacts of simultaneous operating faults on cooling performance of a high efficiency residential heat pump. Energy Build 2021;242:110975.
[35] IPCC. Technical summary. In: climate change 2013: the physical science basis. Cambridge, United Kingdom and New York, United States: Cambridge University Press; 2013.
[36] van Rossum G, Drake FL. *Python 3.6.9 reference manual*, CreateSpace, Scotts Valley. 2019.
[37] U.S. Department of Energy (DOE). EnergyPlus version 9.3 input output reference. Washington, D.C., United States: DOE; 2020.
[38] Deru M, Field K, Studer D, Benne K, Griffith B, Torcellini P, Liu B, Halverson M, Winiarski D, Rosenberg M, Yazdanian M, Huang J, Crawley D, U.S.. Department of Energy commercial reference building models of the national building stock. Golden, United States: National Renewable Energy Laboratory; 2011.
[39] Fumo N, Mago P, Luck R. Methodology to estimate building energy consumption using EnergyPlus Benchmark Models. Energy Build 2010;42(12):2331–7.
[40] Huang S, Ye Y, Wu D, Zuo W. An assessment of power flexibility from commercial building cooling systems in the United States. Energy 2021;221:119571.
[41] Zhang Y, Tennakoon T, Chan YH, Chan KC, Fu SC, Tso CY, Yu KM, Huang BL, Yao SH, Qiu HH, Chao CYH. Energy consumption modelling of a passive hybrid system for office buildings in different climates. Energy 2022;239:121914.
[42] Hoyt T, Arens E, Zhang H. Extending air temperature setpoints: simulated energy savings and design considerations for new and retrofit buildings. Build Environ 2015;88:89–96.
[43] Raman AP, Anoma MA, Zhu L, Rephaeli E, Fan S. Passive radiative cooling below ambient air temperature under direct sunlight. Nature 2014;515:540–4.
[44] Granderson J, Lin G, Harding A, Im P, Chen Y. Building fault detection data to aid diagnostic algorithm creation and performance testing. Sci Data 2020;7(No. 65).
[45] ASHRAE. ASHRAE weather data 2017. Atlanta, United States: ASHRAE; 2017.
[46] Integrated Environmental Solutions (IES), *ApacheHVAC user guide*. Glasgow, United Kingdom: IES; 2016.
[47] Remund J, Müller S, Schmutz M, Barsotti D, Graf P, Cattin R. Meteonorm handbook part I: software. Switzerland: METEOTEST, Bern; 2020.
[48] Eames M, Kershaw T, Coley D. On the creation of future probabilistic design weather years from UKCP09. Build Serv Eng Res Technol 2011;32(Issue 2):127–42.
[49] IPCC, *Global Climate Projections*. In: climate change 2007: the physical science basis. Cambridge, United Kingdom and New York, United States: Cambridge University Press; 2007.
[50] U.S. Department of Energy (DOE). EnergyPlus version 9.3 engineering reference. Washington, D.C., United States: DOE; 2020.

[51] Walton GN. Thermal analysis research program reference manual. Gaithersburg, United States: National Bureau of Standards; 1983.
[52] Fanger PO. Thermal comfort: analysis and applications in environmental engineering. Copenhagen, Denmark: Danish Technical Press; 1970.
[53] Waddicor DA, Fuentes E, Sisó L, Salom J, Favre B, Jiménez C, Azar M. Climate change and building ageing impact on building energy performance and mitigation measures application: a case study in Turin, northern Italy. Build Environ 2016;102:13–25.
[54] Kharseh M, Altorkmany L, Al-Khawaj M, Hassani F. Warming impact on energy use of HVAC system in buildings of different thermal qualities and in different climates. Energy Convers Manag 2014;81:106–11.